A Novel Mathematical Modelling Platform for Evaluation of a Novel Biorefinery Design with Green Hydrogen Recovery to Produce Renewable Aviation Fuel

Jhuma Sadhukhan[*1] and Sohum Sen[1,2]

[1]Centre for Environment and Sustainability, University of Surrey, Guildford, Surrey GU2 7XH, United Kingdom

[2]Computer Science Department, University College London, Gower Street, London WC1E 6BT, United Kingdom

Abstract

A novel integrated biorefinery system consists of 1) pyrolysis of biomass into gas, bio-oil and char; 2) bio-oil hydrodeoxygenation and hydrocracking (hydroprocessing) producing renewable jet fuel and small chain alkanes; 3) alkane steam reforming and pressure swing adsorption (PSA) producing green hydrogen and carbon monoxide; 4) mixed ionic electronic conducting membrane (MIEC) splitting high pressure superheated steam (HPSS) into green hydrogen and oxygen; and 5) combined heat and power generation (CHP) using pyrolysis gas and carbon monoxide from PSA as fuel with oxygen from MIEC, to fulfil the demand for HPSS and electricity. Comprehensive mathematical models are shown for the design simulation of the integrated system: 1) kinetic model of biomass slow and fast pyrolysis at temperature 300-500°C, 2) stoichiometric chemical reaction model of hydroprocessing, 3) renewable aviation fuel property correlations from its chemical compositions for the ASTM D7566 standard, 3) mass and energy balance analyses of the integrated biorefinery system. Economic value and overall avoided environmental and social impacts have been analysed for sustainability. The ratios of mass and energy flowrates between biomass, bio-oil, renewable jet fuel, CHP-fuel, char and hydrogen are 1.33:1:0.45:0.3:0.16:0.05 and 1:0.82:0.7:0.41:0.14:0.22, respectively. For 10tph bio-oil processing, the capital cost of the plant is $14million, the return on investment

[*] Email: jhumasadhukhan@gmail.com

25   is 19% and the cost of production of renewable jet fuel is $0.07/kg, which is lower than its

26   market price, $0.27/kg. This production can curb 108 kt CO_2 equivalent and 1.44 PJ fossil

27   energy per annum. To enable the biorefinery simulation, user-friendly open-source

28   TESARREC™ https://tesarrec.web.app/sustainability/bio-jet-fuel has been developed.

29   **Keywords:** Sustainable aviation fuel from biomass (SAF), net zero greenhouse gas emissions,

30   renewable energy directive, green hydrogen economy, techno-economic analysis and LCA,

31   computer-aided process design and integration

32   **Nomenclature**

33   **Variables for kinetic modelling of biomass pyrolysis**

34   A Arrhenius equation parameter for $k_2 = k_0 \exp\left(-\frac{A}{RT}\right)$

35   k_0 Arrhenius equation parameter for $k_2 = k_0 \exp\left(-\frac{A}{RT}\right)$

36   k_1 rate constant producing gas from biomass pyrolysis (primary reactions)

37   k_2 rate constant for producing bio-oil from biomass pyrolysis (primary reactions)

38   k_3 rate constant for producing char from biomass pyrolysis (primary reactions)

39   k_4 rate constant for the secondary reactions converting bio-oil from the primary reactions

40   into gas and bio-oil

41   $m_B(t)$ mass fraction as a function of time (t) of biomass

42   $m_G(t)$ mass fraction as a function of time (t) of gas

43   $m_O(t)$ mass fraction as a function of time (t) of bio-oil

44   $m_C(t)$ mass fraction as a function of time (t) of char

45   $m_{C,\infty}$ mass fraction of char in steady state conditions

46   R ideal gas constant, 8.314 J mol^{-1}

47   T reaction temperature in K

48   **Variables for mass balance analyses**

49	*Aceticacid*	mass flowrate of acetic acid in bio-oil
50	*AlkanestoReforming*	mass flowrate of alkanes formed in hydroprocessing
51		(hydrodeoxygenation and hydrocracking) reactions and reacted
52		in steam reforming reaction
53	*Bcyclohexane*	mass flowrate of n-butylcyclohexane in renewable jet fuel
54	*Bicyclohexyl*	mass flowrate of bicyclohexyl in renewable jet fuel
55	*BiooilThroughput*	mass flowrate of bio-oil as the basis of mass balance analyses in
56		the proposed model
57	*Cisdecalin*	mass flowrate of cis-decalin in renewable jet fuel
58	*COtoCHP*	mass flowrate of CO from PSA to CHP
59	*Dextrose*	mass flowrate of dextrose in bio-oil
60	*Diamantane*	mass flowrate of diamantane in renewable jet fuel
61	*Diphenyl*	mass flowrate of diphenyl in renewable jet fuel
62	*Dmebenzene*	mass flowrate of 1,2-dimethyl-3-ethylbenzene in renewable jet
63		fuel
64	*ExcessSteam*	mass flowrate of excess steam produced from the site to export
65	*Formicacid*	mass flowrate of formic acid in bio-oil
66	*Furfural*	mass flowrate of furfural in bio-oil
67	*Heptane*	mass flowrate of n-heptane in renewable jet fuel
68	*HydrogenfromReforming*	mass flowrate of hydrogen produced from alkane steam
69		reforming
70	*HydrogenfromSteam*	mass flowrate of hydrogen needed to be produced by MIEC
71	*HydrogenNeeded*	mass flowrate of hydrogen needed in hydroprocessing
72		(hydrodeoxygenation and hydrocracking) reactions
73	*Hydroxyacetone*	mass flowrate of hydroxyacetone in bio-oil

74	*Mcyclohexane*	mass flowrate of methylcyclohexane in bio-oil
75	*MIECFeed*	mass flowrate of steam fed to MIEC
76	*OxygenfromSteam*	mass flowrate of oxygen produced from MIEC
77	*Pcyclohexane*	mass flowrate of n-propylcyclohexane in renewable jet fuel
78	*Phenol*	mass flowrate of phenol in bio-oil
79	*PhenoltoTridecene1*	fractional reaction conversion of phenol into 1-tridecene in
80		Reaction 1 in Equation 5
81	*PhenoltoTridecene2*	fractional reaction conversion of phenol into 1-tridecene in
82		Reaction 7 in Equation 5
83	*Pxylene*	mass flowrate of p-xylene in renewable jet fuel
84	*SteamProduced*	mass flowrate of steam produced in hydroprocessing
85		(hydrodeoxygenation and hydrocracking) reactions
86	*Thnaphthalene*	mass flowrate of 1,2,3,4-tetrahydronaphthalene in renewable jet
87		fuel
88	*Tmbenzene*	mass flowrate of 1,2,3-trimethylbenzene in renewable jet fuel
89	*Tmcyclohexane*	mass flowrate of 1-*trans*-3,5-trimethylcyclohexane in renewable
90		jet fuel
91	*Tmheptane*	mass flowrate of 3,3,5-trimethylheptane in renewable jet fuel
92	*Tridecene*	mass flowrate of 1-tridecene in renewable jet fuel
93	*Triethylbenezene*	mass flowrate of 1,2,4-triethylbenzene in renewable jet fuel
94	*Water*	mass flowrate of water present in bio-oil
95	*Xylenol*	mass flowrate of 2,5-xylenol in renewable jet fuel
96		

Introduction

The COP26 summit is aimed at accelerating actions towards the goals of the Paris Agreement and the UN Framework Convention on Climate Change to meet the net zero greenhouse gas emissions target (COP26, 2021). Biorefineries can attain net zero or even carbon negative targets by displacing fossil-carbon based economy (Sy et al., 2018; Leong et al., 2019), by the provision of food, personal and home care products, and energy and water services, while effectively responding to changing supply and demand conditions and offering economic feasibility and life cycle sustainability (Sadhukhan et al., 2018; Sadhukhan et al., 2019). Sustainable biomass is wastes, residues, and non-food cellulosic and lignocellulosic feedstocks, which can avoid conflicts with food or feed production, and land use for forestation (Popp et al., 2014; Nanda et al., 2015). These are categorised into five different groups 1) agricultural and forestry residues, 2) garden wastes: leaves, green plant materials, grass silage, empty fruit bunch, immature cereals, 3) oily residues: waste cooking oils and animal fat, 4) aquatic biomass: algae and seaweed, and 5) organic residues: municipal waste, manure and sewage (Sadhukhan et al., 2014). Amongst these, lignocellulosic biomass is the most abundant (Cai et al., 2017). Lignocellulosic biomass consisting of cellulose (38-54% by mass), hemicellulose (24-36%) and lignin (15-25%) can be found in plant cell walls (Sadhukhan et al., 2014; Sadhukhan et al., 2020) and thus in agricultural, forestry, garden, and food wastes (Ebikade et al., 2020; Wang et al., 2021).

A biorefinery must be an integrated industrial system embedding process systems engineering or process integration (Ng et al., 2015) for high-efficiency flexible conversion of biomass feedstocks into multiple added-value products (Sadhukhan et al., 2014; El-Halwagi, 2017). Process integration allows meeting all material and energy resource needs by thermodynamic matching between source and sink processes within the biorefinery system (Dimian et al., 2014; Leong et al., 2019). This makes the integrated biorefinery system robust and self-sustainable

122   least reliant on external supplies. The best way to design and evaluate an optimal integrated

123   sustainable biorefinery system is by computer-aided mathematical modelling of the entire

124   system (Ling et al., 2019; Gutiérrez-Antonio et al., 2020).

125   The aviation sector is in desperate need of renewable fuels for greenhouse gas negative or

126   neutral performance (Zhang et al., 2020). For example, in the UK, in 2019, the entire energy

127   demand of air transport is met from fossil resources (BEIS, 2021). Sustainable aviation fuel

128   (SAF) can be produced from sustainable biomass in an integrated self-sustainable biorefinery

129   system. The biorefinery design must be sustainable to effectively replace petroleum refineries.

130   To date, the literature has focused on the core reactions. The recovery of green hydrogen,

131   oxygen, heat and electricity within the biorefinery to meet or exceed their demands for

132   producing SAF has largely been neglected. To close this gap, this research develops a novel

133   integrated self-sustainable biorefinery system with the in-process recovery of green hydrogen,

134   oxygen, heat and electricity etc. to meet or exceed their demands to produce SAF.

135   The two SAF producing technologies supported by the ASTM D7566 standard (ASTM D7566,

136   2020) are based on the Fischer-Tropsch liquid (FT) synthesis (Ng and Sadhukhan, 2011) and

137   hydroprocessing technologies (Sadhukhan and Ng, 2011; Liu et al., 2017). Sustainable biomass

138   that can be processed through these two technologies includes lignocelluloses and oily residues.

139   FT synthesis, invented in the early 20th century, is operated at a large scale to transform gas or

140   solid into liquid fuel (Sadhukhan et al., 2014). Compared to the FT synthesis process, the

141   hydroprocessing technologies offer more flexibility in terms of the scale of operation and type

142   of biomass feedstock (Zacher et al., 2014; Romero-Izquierdo et al., 2021), which are important

143   due to the difficulty of its transport logistics over long distances and seasonality affecting its

144   available quantity and quality (Sadhukhan et al., 2014). Self-sustainability of the

145   hydroprocessing technologies is an intriguing challenge because of its high hydrogen demand

146   to make SAF or renewable jet fuel. Only less than half of the total hydrogen need of

147 hydroprocessing can be met by steam reforming of alkanes from hydroprocessing (Sadhukhan

148 and Ng, 2011). The remaining hydrogen requirements are met from crude oil refinery through

149 blue or grey hydrogen sourcing (Jones et al., 2009; Zacher et al., 2014). More recent

150 publications have considered external hydrogen import for hydroprocessing (Martinez-

151 Hernandez et al., 2019; Romero-Izquierdo et al., 2021). These processes are inevitable to fail

152 economically and environmentally if they are to buy (blue or grey) hydrogen (and energy) from

153 fossil resources to fulfil their demands. This is the main bottleneck to the industrial uptake of

154 the technology despite the legislative pull. This paper shows a compelling novel integrated

155 biorefinery case by its inherent sustainability through in-process green hydrogen and energy

156 integration for the industry.

157 This research aims to offer many distinguishing fundamental scientific contributions

158 embedding green chemistry, process integration including intensification, and circular

159 economy principles. The new processes added to largely hydroprocessing-focused

160 configurations are a *combined heat and power system* (CHP) and *an intensified mixed ionic*

161 *electronic conducting membrane process* (MIEC). The CHP runs on offgas containing carbon

162 monoxide from *pressure swing adsorption* (PSA) separating hydrogen from alkane steam

163 reforming and pyrolysis gas to generate high pressure superheated steam for the reforming and

164 MIEC. MIEC meets the remaining hydrogen requirements of the site (greater than half) by

165 splitting high pressure superheated steam into green hydrogen and oxygen. Oxygen is the

166 oxidant for the boiler of the CHP. The green hydrogen sourced entirely from biomass is

167 consumed by hydroprocessing to make the SAF. To the best of the authors' knowledge, this is

168 the first publication on a fully integrated self-sufficient novel renewable aviation fuel-

169 producing biorefinery system and its comprehensive mathematical models for its design

170 simulation under different conditions.

171   The paper is structured as follows. The following section discusses the deduction of a robust

172   generic kinetic model of biomass pyrolysis process based on slow and fast pyrolysis product

173   distributions within the 300-500°C temperature. The development of the mass and energy

174   balance equations using chemical reaction stoichiometries and renewable jet fuel property

175   correlations from its constituent chemical compositions are then discussed. The final section

176   of the methodology discusses a comprehensive economic value analysis methodology

177   (Martinez-Hernandez et al., 2013; Martinez-Hernandez et al., 2014), and an overall impact

178   assessment based on life cycle assessment (LCA) (Kolosz et al., 2020) and social life cycle

179   assessment (SLCA) (Shemfe et al., 2018; Sadhukhan et al., 2021). There are two reasons for

180   opting out of detailed life cycle sustainability assessment, for which readers are directed to

181   Sadhukhan et al. (2019) and Sadhukhan et al. (2021): 1) the focus of this research is the design

182   of the integrated biorefinery system, 2) the life cycle impacts reside with the external energy

183   and hydrogen supplies which are eliminated by the 'process integration' of the biorefinery

184   system. The final sections include results and discussions, and conclusions of this research.

185   **Methodology**

186   This section first discusses the novel integrated biorefinery configuration and then

187   comprehensive models for biomass pyrolysis kinetic, hydroprocessing reaction and renewable

188   jet fuel property models, mass and energy balance around steam reforming, PSA, CHP and

189   MIEC, and economic value and overall sustainability analyses.

190   Fig. 1 shows the novel integrated biorefinery configuration developed in this research. The

191   inset table shows the various mathematical modelling aspects at the unit process or system

192   level. The decanter and distillation train can be noted in Fig. 1. These are to separate lighter

193   alkanes from the final renewable jet fuel product (>C7) from hydroprocessing that occurs in

194   two reaction series: hydrodeoxygenation and hydrocracking. Process simulation of

hydroprocessing and decanter + distillation train is detailed elsewhere (Sadhukhan and Ng,

2011) and outlined in Appendix A.
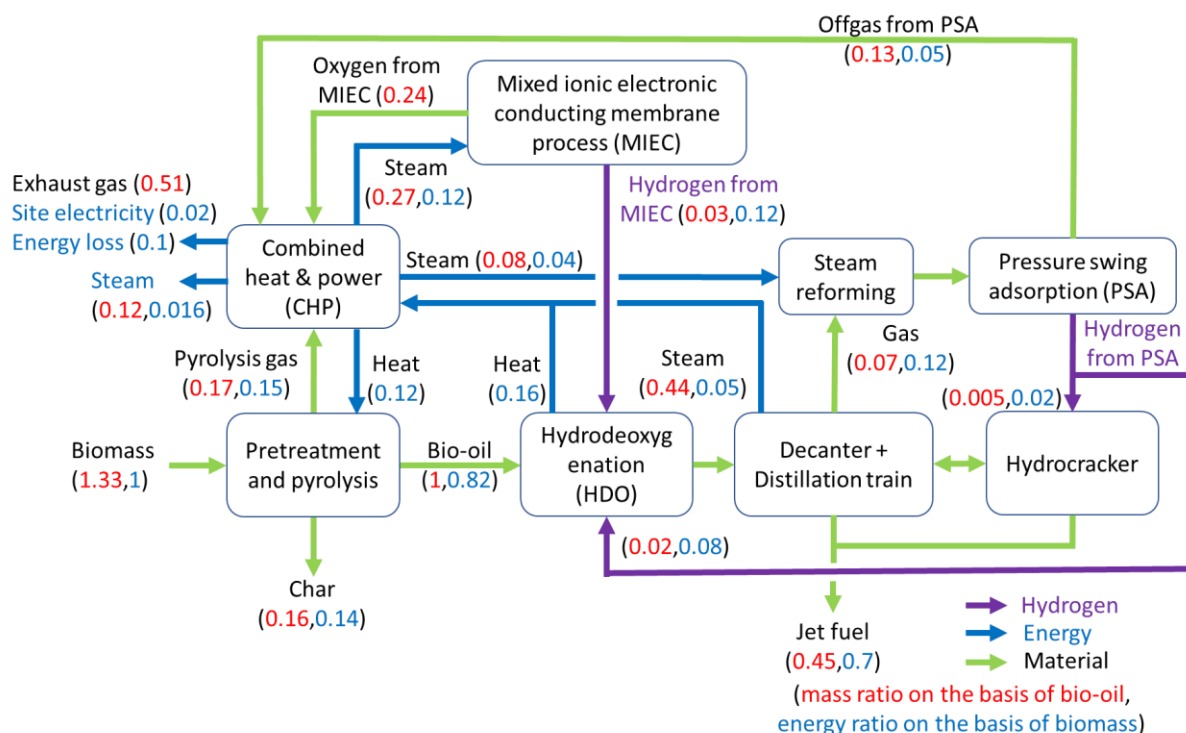
Technical modelling basis	Unit process
Kinetic modelling	Biomass pyrolysis
Reaction stoichiometry analyses	Hydroprocessing
Property correlations from composition	Renewable jet fuel for ASTM D7566
Mass and energy balance, economic value, and sustainability analyses	Integrated biorefinery system

Fig. 1 Novel integrated biorefinery design. The inset table shows the modelling bases.

The novel biorefinery configuration consists of biomass pyrolysis into bio-oil, gas and char

productions; bio-oil hydroprocessing into renewable jet fuel production; on-site hydrogen

203   resourcing by alkane steam reforming followed by PSA and MIEC; CHP using pyrolysis gas

204   and PSA offgas, and oxygen from MIEC, as shown in Fig. 1.

205   **Kinetic modelling of biomass pyrolysis**

206   Pyrolysis is a thermal conversion reaction of organics into liquid in the absence of oxygen.

207   This process occurs at a temperature of around 300-700°C. This is a thermal degradation

208   process, where large molecules are decomposed into smaller fragments, producing bio-oil from

209   the middle, gas from the top and char from the bottom. Bio-oil is an important platform

210   feedstock for chemicals and fuels.

211   A generic and robust kinetic model of biomass pyrolysis between temperatures 300°C and

212   500°C is shown in this section to estimate the distributions of pyrolysis products, i.e. pyrolysis

213   gas, bio-oil and char. The Waterloo kinetic model (Liden et al., 1988; Yang et al., 2018)

214   parameters are estimated within the given operating range. The parameters are estimated based

215   on the same product distributions observed at two boundary conditions, 300°C and 500°C in

216   the literature (see, for example, Jahirul et al., 2012; Musa, 2017). The char, bio-oil and gas

217   product distributions of biomass pyrolysis under these two conditions are shown in Table 1.

218   The Waterloo model is a generic pyrolysis reaction model that considers pyrolysis reactions in

219   a two-stage mechanism (Liden et al., 1988). The primary reactions involve the formation of

220   gas, oil, and char. The secondary reactions involve the conversion of oil into further gas, oil,

221   and char. The secondary conversion of bio-oil into char is negligible. Fig. 2 shows the Waterloo

222   concept, based on which, the mass transfer equations for biomass, gas, bio-oil and char are

223   developed, as shown in Equation 1 (Sadhukhan et al., 2014).

k_1 → Gas 1 (G)
k_2 → Oil 1 (O)
k_3 → Char 1 (C)
k_4 → Gas 2 / Oil 2 / Char 2

Biomass (B)

Primary reactions   Secondary reactions

224
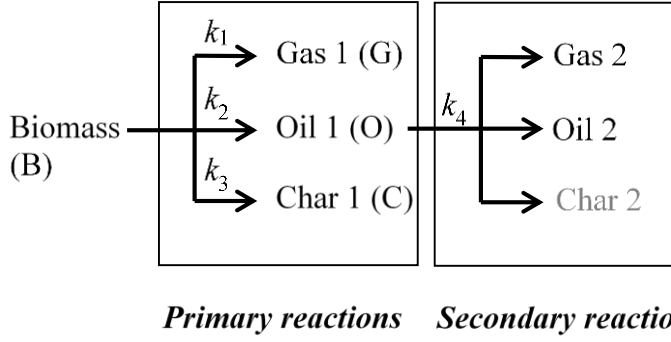
225   **Fig. 2** The Waterloo concept for modelling biomass pyrolysis reaction system.

226    $$\frac{dm_B(t)}{dt} = -(k_1 + k_2 + k_3)m_B(t) = -km_B(t)$$

227    $$\frac{dm_G(t)}{dt} = k_1 m_B(t) + k_4 m_O(t)$$

228    $$\frac{dm_O(t)}{dt} = k_2 m_B(t) - k_4 m_O(t)$$

229    $$\frac{dm_C(t)}{dt} = k_3 m_B(t)$$

230   At $t = 0$, $m_B(t) = 1$ and $m_G(t) = m_O(t) = m_C(t) = 0$ \hfill Equation 1

231    $m_B(t), m_G(t), m_O(t), m_C(t)$ are the mass fractions as a function of residence time (t) of

232   biomass, gas, bio-oil, and char. k_1 is the rate constant producing gas from biomass. k_2 is the

233   rate constant for producing bio-oil from biomass. k_3 is the rate constant for producing char

234   from biomass. These reaction steps make up the primary reactions. The rate constant for the

235   secondary reactions converting bio-oil from the primary reactions into gas and bio-oil from the

236   secondary reactions is k_4. The initial condition and the mass transfer equations, shown in

237   Equation 1, make the problem an initial value problem (IVP). The rate constant expressions,

238   k_1, k_3 and k_4 are also obtained from the Waterloo model, as in Equation 2. Introduction of

239   Equation 2 makes the equations' system an IVP differential algebraic equation (DAE) system.

240   The expressions for k_1 and k_4 correspond to the Arrhenius equation. R is the ideal gas constant,

241 8.314 J mol^{-1}. T is the reaction temperature in K. $m_{C,\infty}$ is the mass fraction of char in steady

242 state conditions.

243 $k_1 = 14300\exp\left(\dfrac{-106500}{RT}\right)$

244 $k_3 = \dfrac{m_{C,\infty}}{1 - m_{C,\infty}}(k_1 + k_2)$

245 $k_4 = 7900\exp\left(\dfrac{-81000}{RT}\right)$

246 $k = (k_1 + k_2 + k_3)$ Equation 2

247 Furthermore, the equation system can be transformed into a boundary value problem by

248 introducing the concentration obtained in the reactions at the two temperatures 300°C and

249 500°C. Table 1 shows the steady state product concentrations (gas, oil and char) from slow and

250 fast pyrolysis reactions at the two temperatures, respectively (Jahirul et al., 2012; Mofijur et

251 al., 2019).

252 Table 1. Biomass pyrolysis product distributions at two temperatures.

300°C	$m_G = 0.35$	$m_O = 0.3$	$m_C = 0.35$
500°C	$m_G = 0.13$	$m_O = 0.75$	$m_C = 0.12$

253

254 The analytical expressions for $m_B(t), m_G(t), m_O(t), m_C(t)$ were obtained by solving

255 Equations 1-2 in the previous work (Sadhukhan et al., 2014), as shown in Equation 3.

256 $m_B(t) = \exp(-kt)$

257 $m_G(t) = -\dfrac{k - k_4}{k}[kk_1 \exp(-kt)$

258         $- k_1 k_4 \exp(-kt) - k_2 k_4 \exp(-kt) + kk_2 \exp(-k_4 t) - kk_1 + k_1 k_4 + k_2 k_4$

259         $- kk_2$

260 $m_O(t) = -\dfrac{k_2}{k - k_4}\exp(-k_4 t)[\exp(-t(k - k_4)) - 1]$

12

261     $m_C(t) = \frac{k_3}{k}[1 - \exp(-kt)]$ Equation 3

262   There are 8 expressions (Equations 2-3) for $m_B(t), m_G(t), m_O(t), m_C(t), k_1, k_3, k_4, k$. There

263   are nine variables: $m_B(t), m_G(t), m_O(t), m_C(t), k_1, k_2, k_3, k_4, k$. Such a problem can be solved

264   using an optimisation method suitable for non-linear programming. The problem can be solved

265   using the generalised reduced gradient (GRG) method. The details of the GRG method are

266   shown elsewhere (Sadhukhan et al., 2014). Equations 2-3 are solved using the GRG method

267   applying the boundary values shown in Table 1. Fig. 3 shows the solution in terms of unsteady

268   state mass fractions of biomass, pyrolysis gas, bio-oil, and char. It can be seen from the

269   unsteady state plots in Fig. 3 that after about 2500 and 6 seconds, the steady state distributions

270   are reached in the slow and fast biomass pyrolysis, respectively. The values of k_2 obtained at

271   the two temperatures 300°C and 500°C are 0.63 and 0.91, respectively.

$m_{C,\infty} = 0.35$ $m_{C,\infty} = 0.12$

Optimisation solution	k_1	0	$k_1 = 14300 \exp\left(\dfrac{-106500}{RT}\right)$	k_1	0.000909	Optimisation solution
	k_2	0.626104		k_2	0.910470	
	k_3	0.337135	$k_3 = \dfrac{m_{C,\infty}}{1 - m_{C,\infty}}(k_1 + k_2)$	k_3	0.124279	
	k_4	0.000326		k_4	0.026543	
	k	0.963242	$k_4 = 7900 \exp\left(\dfrac{-81000}{RT}\right)$	k	1.035657	

272
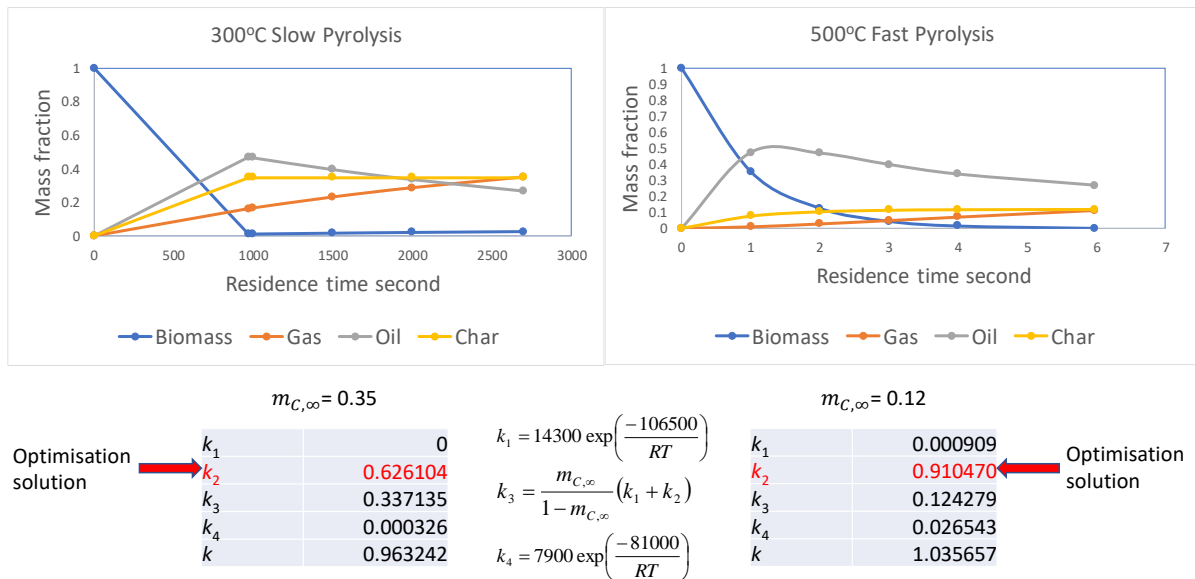
273   **Fig. 3** Biomass pyrolysis reaction kinetic modelling results and parameters (temperature: 300-

274   500°C).

275   Furthermore, the Arrhenius equation parameters for k_2 are obtained as shown in Equation 4.

276   The linear correlation between $\ln k_2$ and $\left(-\frac{1}{T}\right)$ based on two data points ($k_2 = 0.626$ at $T =$

277   573K; and $k_2 = 0.91$ at $T = 773K$) gives the Arrhenius equation parameters for k_2, $k_0 =$

278   2.6618 and $A = 6894.4676$.

279   $k_2 = k_0 \exp\left(-\frac{A}{RT}\right)$

280   $\ln k_2 = \ln k_0 + \frac{A}{R}\left(-\frac{1}{T}\right)$

281   $k_2 = 2.6618 \exp\left(-\frac{6894.4676}{RT}\right)$ Equation 4

282   Thus, Equations 2-4 describe the biomass pyrolysis kinetics from which the steady state

283   product concentrations can be determined at 300-500°C. The results are in good agreement

284   with the literature that suggests the universal nature of biomass pyrolysis performance in terms

285   of the proportions of the gas, bio-oil and char products depending upon the temperature (Jahirul

286   et al., 2012; Ranzi et al., 2017). The Waterloo kinetic model described in Fig. 2 and Equations

287   1-3 can be applied for different temperature ranges. In this case, the model is presented only

288   for a temperature range of 300-500°C suitable for the biorefinery system under consideration.

289   **Hydroprocessing reaction and renewable jet fuel property models**

290   Bio-oil produced from biomass pyrolysis needs to be stabilised by oxygen removal from 35-

291   40% to less than 2% by mass of bio-oil. This requires hydrodeoxygenation of bio-oil into stable

292   bio-oil. Hydrodeoxygenation reaction is the removal of oxygen by hydrogen addition in the

293   form of water. Some decarboxylation reactions may occur, which is the removal of oxygen via

294   carbon dioxide or carbon monoxide formation. Stable oil from hydrodeoxygenation requires

295   hydrocracking including isomerisation. Thus, hydroprocessing occurs in two reaction series:

296   hydrodeoxygenation and hydrocracking.

297   This section first shows the balanced reaction equations between bio-oil and renewable jet fuel

298   components. These reactions occur in hydrodeoxygenation (Reactions 1-37) and

299   hydrocracking (Reactions 38-40) reactors, shown in Equation 5. Forty reaction steps between

300   bio-oil and renewable jet fuel chemical constituents, applying ring separation, ring opening,

cracking, saturation and isomerisation reaction mechanisms, were deduced by linear regression

(Sadhukhan and Ng, 2011), to accurately match with the product profiles by Jones et al. (2009).

The bio-oil components are phenol, dextrose, furfural, acetic acid, hydroxyacetone and formic

acid (Jones et al., 2009). Table 2 shows the renewable jet fuel constituent chemicals and

properties. The renewable jet fuel constituent chemicals in Table 2 are found in tested jet fuel

or green diesel fractions from bio-oil hydroprocessing or are found to be blended to make a

drop-in jet fuel (Jones et al., 2009; Harvey et al., 2015). Their significance in making up a

sustainable aviation fuel can be seen from their Fourier-transform infrared spectroscopy (FTIR)

in the literature in the context of renewable fuel blending (see e.g. SpectraBase™). These are

thus the more realistic target chemicals in drop-in renewable jet fuel.

Equation 5 shows the specific conversions of reactants in the various reactions to meet the

renewable jet fuel ASTM D7566 standard. Reaction 1 and 7 conversions strongly influence the

jet fuel properties. 1-tridecene is formed from phenol in these two reactions. A higher 1-

tridecene fraction in renewable jet fuel enhances its ASTM D7566 standard. 1-tridecene has

been a target molecule in renewable jet fuel (Martinez, 2021). This also demands closer

scrutiny of the renewable jet fuel property correlations from its constituent chemical

compositions shown in this research.

The conversions of phenol, present in bio-oil, in the various reactions, are dependent on

$PhenoltoTridecene1$ and $PhenoltoTridecene1$, fractional conversions of phenol in

Reactions 1 and 7, respectively. This is because 1-tridecene produced in Reactions 1 and 7 has

superior ASTM D7566 properties and thus should be a target component in renewable jet fuel.

However, at the same time, if its concentration in the renewable jet fuel product is too high, it

can adversely affect the product properties. All components of renewable jet fuel thus need to

be carefully controlled to meet the ASTM D7566 standards. The balance of fractional

conversions of phenol $(1 - PhenoltoTridecene1 - PhenoltoTridecene2)$ accounts for

326 conversions of phenol in its all other reactions. The fractional conversions of phenol in

327 Reactions 2-6 and 8-15 out of a total of $(1 - PhenoltoTridecene1 - PhenoltoTridecene2)$

328 are the same as in our earlier studies (Sadhukhan and Ng, 2011; Sadhukhan et al., 2014).

329 **Reactions of phenol:**

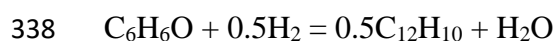330 Reaction 1: Hydrodeoxygenation (HDO) to 1-tridecene:

331 $C_6H_6O + 4H_2 = 0.46C_{13}H_{26} + H_2O$ (Conversion (fractional) of phenol in this research:

332 $PhenoltoTridecene1$)

333 Reaction 2: Dehydroxygenation to chrysene:

334 $C_6H_6O = 0.33C_{18}H_{12} + H_2O$
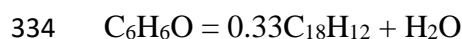
335 Reaction 3: HDO to diamantane:

336 $C_6H_6O + 2.29H_2 = 0.43C_{14}H_{20} + H_2O$

337 Reaction 4: HDO to diphenyl:

338 $C_6H_6O + 0.5H_2 = 0.5C_{12}H_{10} + H_2O$

339 Reaction 5: HDO to isobutane and phenanthrene:

340 $C_6H_6O + 1.33H_2 = 0.33C_4H_{10} + 0.33C_{14}H_{10} + H_2O$
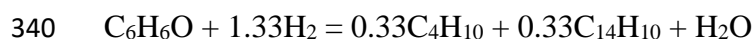
341 Reaction 6: HDO to 1,2,4-triethylbenzene:

342 $C_6H_6O + 2.5H_2 = 0.5C_{12}H_{18} + H_2O$

343 Reaction 7: HDO to 1-tridecene, phenanthrene, n-heptane and ethane:

344 $C_6H_6O + 2.83H_2 = 0.167C_{13}H_{26} + 0.167C_{14}H_{10} + 0.167C_7H_{16} + 0.167C_2H_6 + H_2O$
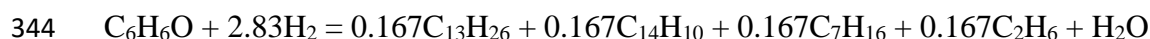
345   (Conversion: $PhenoltoTridecene2$)

346 Reaction 8: HDO to 1-*trans*-3,5-trimethylcyclohexane:

347 $C_6H_6O + 4H_2 = 0.67C_9H_{18} + H_2O$
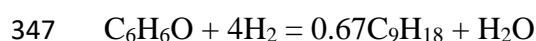
348 Reaction 9: HDO to n-propylcyclohexane:

349 $C_6H_6O + 4H_2 = 0.67C_9H_{18} + H_2O$
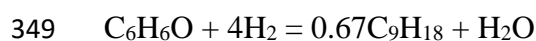
350 Reaction 10: HDO to p-xylene:

351    $C_6H_6O + 1.75H_2 = 0.75C_8H_{10} + H_2O$

352   Reaction 11: HDO and decarboxylation (DCO) to 1-tridecene and isobutane:

353    $C_6H_6O + 3.33H_2 = 0.33C_{13}H_{26} + 0.33C_4H_{10} + 0.33CO_2 + 0.33H_2O$
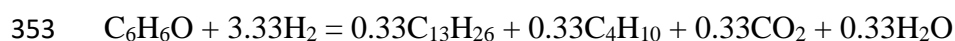
354   Reaction 12: HDO to bicyclohexyl:

355    $C_6H_6O + 3.5H_2 = 0.5C_{12}H_{22} + H_2O$

356   Reaction 13: HDO to 2,5-xylenol:

357    $C_6H_6O + H_2 = 0.75C_8H_{10}O + 0.25H_2O$
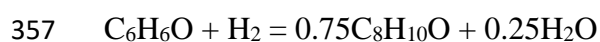
358   Reaction 14: HDO to 1,2,3-trimethylbenzene:

359    $C_6H_6O + 2H_2 = 0.67C_9H_{12} + H_2O$
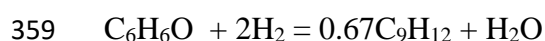
360   Reaction 15: HDO to n-heptane, isobutane and methane:

361    $C_6H_6O + 5.5H_2 = 0.5C_7H_{16} + 0.5C_4H_{10} + 0.5CH_4 + H_2O$

362   **Reactions of dextrose:**

363   Reaction 16: HDO to 2,5-xylenol:

364    $C_6H_{12}O_6 + 3H_2 = 0.75C_8H_{10}O + 5.25H_2O$ (Conversion (fractional) of dextrose in this research:

365   0.376)
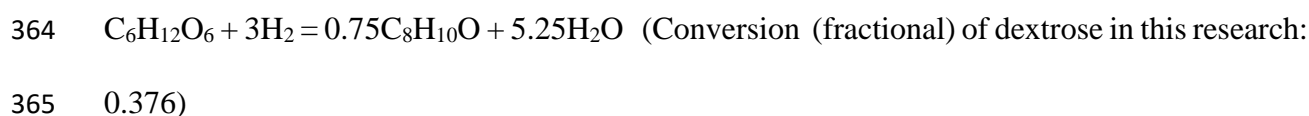
366   Reaction 17: HDO and DCO to diamantane:

367    $C_6H_{12}O_6 + 0.67H_2 = 0.33C_{14}H_{20} + 1.33CO_2 + 3.33H_2O$ (Conversion: 0.196)
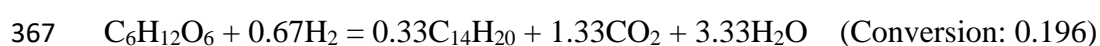
368   Reaction 18: HDO and DCO and methane production:

369    $C_6H_{12}O_6 + 8H_2 = 5CH_4 + CO_2 + 4H_2O$ (Conversion: 0.124)
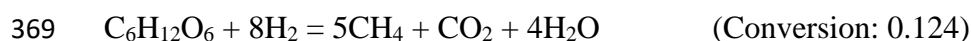
370   Reaction 19: HDO to 1-*trans*-3,5-trimethylcyclohexane:

371    $C_6H_{12}O_6 + 6H_2 = 0.67C_9H_{18} + 6H_2O$ (Conversion: 0.094)
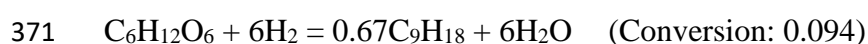
372   Reaction 20: HDO to n-propylcyclohexane:

373    $C_6H_{12}O_6 + 6H_2 = 0.67C_9H_{18} + 6H_2O$ (Conversion: 0.094)

374   Reaction 21: HDO and DCO to 1,2,3-trimethylbenzene:

375    $C_6H_{12}O_6 + 2H_2 = 0.5C_9H_{12} + 0.5CH_4 + CO_2 + 4H_2O$ (Conversion: 0.041)

376   Reaction 22: HDO and DCO to cis-decalin:

377    $C_6H_{12}O_6 + 4.5H_2 = 0.5C_{10}H_{18} + 0.5CH_4 + 0.5CO_2 + 5H_2O$ (Conversion: 0.036)

378   Reaction 23: HDO and DCO to 1-tridecene:

379    $C_6H_{12}O_6 + 2.33H_2 = 0.33C_{13}H_{26} + 0.33CH_4 + 1.33CO_2 + 3.33H_2O$ (Conversion: 0.02)

380   Reaction 24: HDO and DCO to n-butylcyclohexane:

381    $C_6H_{12}O_6 + 5H_2 = 0.5C_{10}H_{20}O + 0.5CH_4 + 0.5CO + 5H_2O$ (Conversion: 0.012)

382   Reaction 25: HDO to bicyclohexyl:

383    $C_6H_{12}O_6 + 5.5H_2 = 0.5C_{12}H_{22} + 6H_2O$ (Conversion: 0.008)
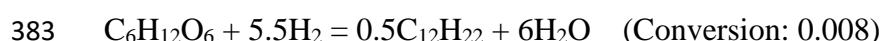
384   **Reactions of furfural:**

385   Reaction 26: HDO to cis-decalin:

386    $C_5H_4O_2 + 4.5H_2 = 0.5C_{10}H_{18} + 2H_2O$ (Conversion (fractional) of furfural in this research:

387   0.313)
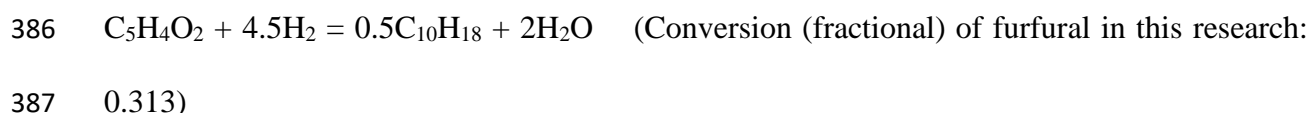
388   Reaction 27: HDO to 3,3,5-trimethylheptane:

389    $C_5H_4O_2 + 5.5H_2 = 0.5C_{10}H_{22} + 2H_2O$ (Conversion: 0.232)
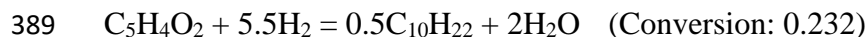
390   Reaction 28: HDO to 1,2-dimethyl-3-ethylbenzene:

391    $C_5H_4O_2 + 3.5H_2 = 0.5C_{10}H_{14} + 2H_2O$ (Conversion: 0.204)

392   Reaction 29: HDO to methane:

393    $C_5H_4O_2 + 10H_2 = 5CH_4 + 2H_2O$ (Conversion: 0.139)
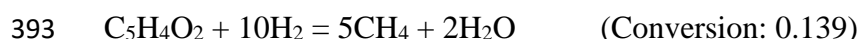
394   Reaction 30: DCO to propane and methane:

395    $C_5H_4O_2 + 4H_2 = C_3H_8 + CH_4 + CO_2$ (Conversion: 0.108)

396   Reaction 31: HDO to n-butylcyclohexane:

397    $C_5H_4O_2 + 5H_2 = 0.5C_{10}H_{20} + 2H_2O$ (Conversion: 0.005)

398   **Reactions of acetic acid:**

399   Reaction 32: HDO and DCO to ethane and methane:

400     $C_2H_4O_2 + 1.5H_2 = 0.5C_2H_6 + 0.5CH_4 + 0.5CO_2 + H_2O$ (Conversion (fractional) of acetic acid

401   in this research: 0.616)

402   Reaction 33: HDO and DCO to alkanes and isoparaffins:

403     $C_2H_4O_2 + 2.22H_2 = 0.11C_7H_{16} + 0.11C_4H_{10} + 0.11C_3H_8 + 0.11C_2H_6 + 0.11CH_4 + 0.11CO_2 +$

404     $1.78H_2O$ (Conversion: 0.384)

405   **Reactions of hydroxyacetone:**

406   Reaction 34: HDO and DCO to alkanes:

407     $C_3H_6O_2 + 2H_2 = 0.25C_7H_{16} + 0.25C_3H_8 + 0.25CH_4 + 0.25CO_2 + 1.5H_2O$ (Conversion

408   (fractional) of hydroxyacetone in this research: 0.966)

409   Reaction 35: HDO to alkane:

410     $C_3H_6O_2 + 5H_2 = 3CH_4 + 2H_2O$ (Conversion: 0.034)

411   **Reactions of formic acid:**

412   Reaction 36: HDO and DCO to alkanes:

413     $CH_2O_2 + 1.75H_2 = 0.25C_2H_6 + 0.25CH_4 + 0.25CO_2 + 1.5H_2O$ (Conversion (fractional) of

414   formic acid in this research: 0.954)

415   Reaction 37: HDO and DCO to alkane:

416     $CH_2O_2 + H_2 = 0.5CH_4 + 0.5CO_2 + H_2O$ (Conversion: 0.046)

417   **Hydrocracking including isomerisation:**

418   Reaction 38: Hydrogenation of phenanthrene to cyclohexane: methylcyclohexane:

419     $C_{14}H_{10} + 9H_2 = 2C_7H_{14}$ (100% conversion in this research)

420   Reaction 39: Hydrogenation of chrysene to cyclohexane: 1-*trans*-3,5-trimethylcyclohexane:

421     $C_{18}H_{12} + 12H_2 = 2C_9H_{18}$ (100% conversion in this research)

422   Reaction 40: Methylcyclohexane to 1,2,3,4-tetrahydronaphthalene and n-butane:

423     $2C_7H_{14} = C_{10}H_{12} + C_4H_{10} + 3H_2$ (10% conversion in this research)   Equation 5

424   The reaction stoichiometries and conversions in Equation 5 generate the mass balance

425   equations for chemicals, as shown in Equation 6. Molar masses of chemicals have been applied

426   for conversions between mass and molar flows as appropriate. The chemical names in Equation

427   6 indicate their mass flowrates (See the Nomenclature). $JetFuel$ is the total of the amounts of

428   the renewable jet fuel chemicals derived from the various mass balance equations.

429     $HydrogenNeeded$, $AlkanestoReforming$ and $SteamProduced$ are also deduced in

430   Equation 6, based on the reaction stoichiometries and conversions in Equation 5.

431     $HydrogenNeeded$, $AlkanestoReforming$ and $SteamProduced$ are further used in mass

432   balance equations around alkane steam methane reforming, PSA, CHP and MIEC, discussed

433   in the next section. Equation 6 is based on the steady state mass balance principle that the mass

434   flowrate of a chemical ($Chemical$) is the difference between its productions and consumptions

435   in the various reaction balance equations, dependent on their stoichiometries and conversions,

436   as follows.

437     $Chemical$

$$438 \quad = \sum_{all\ reactions} (ratio\ of\ stoichiometries\ between\ chemical\ product\ and\ reactant\ in\ reaction$$

439     $\times\ reactant\ molar\ mass\ \times\ chemical\ molar\ mass$

440     $\times\ fractional\ conversion\ of\ the\ reactant\ in\ the\ reaction)$

$$441 \quad - \sum_{all\ reactions} (ratio\ of\ stoichiometries\ between\ chemical\ (reactant) and\ reactant\ in\ reaction$$

442     $\times\ reactant\ molar\ mass\ \times\ chemical\ molar\ mass$

443     $\times\ fractional\ conversion\ of\ the\ reactant\ in\ the\ reaction)$

444   This generic equation is shown for the specific chemicals produced or consumed by

445   hydroprocessing, in Equation 6. The equation for the mass flowrate of chrysene is not shown,

446   because chrysene produced in Reaction 2 is completely reacted in Reaction 39 producing 1-

447 *trans*-3,5-trimethylcyclohexane. The equation for $Tmcyclohexane$ (mass flowrate of 1-*trans*-

448 3,5-trimethylcyclohexane) captures the formation and consumption of chrysene.

449 $PhenoltoTridecene1$ and $PhenoltoTridecene2$, the fractional conversions of phenol into 1-

450 tridecene in Reactions 1 and 7, as discussed earlier, are incorporated as independent variables

451 (rather than fixed values) in Equation 6, because the renewable jet fuel properties are sensitive

452 to these variables. Their feasible ranges for the acceptable renewable jet fuel properties are

453 shown in the results and discussions.

454 As discussed earlier, the fractional conversions of phenol in Reactions 2-6 and 8-15 are

455 $\frac{fractional\ conversion\ in\ earlier\ study}{(1-PhenoltoTridecene1-PhenoltoTridecene2)}$.

456 $Tridecene = ((PhenoltoTridecene1 \times 0.46 + PhenoltoTridecene2 \times 0.167$

457 $+ 0.0065 \times (1 - PhenoltoTridecene1$

458 $- PhenoltoTridecene2) \times 0.33) \times Phenol\ /\ 94$

459 $+ 0.02 \times 0.33 \times Dextrose\ /\ 180) \times 182$

460 $Diamantane = ((0.1766 \times (1 - PhenoltoTridecene1$

461 $- PhenoltoTridecene2) \times 0.4286) \times Phenol\ /\ 94$

462 $+ 0.196 \times 0.3345 \times Dextrose/180) \times 188$

463 $Diphenyl = 0.1390 \times (1 - PhenoltoTridecene1$

464 $- PhenoltoTridecene2) \times 0.5 \times Phenol/94 \times 154$

465 $Triethylbenezene$

466 $= 0.0961 \times (1 - PhenoltoTridecene1$

467 $- PhenoltoTridecene2) \times 0.5 \times Phenol/94 \times 162$

468 $Heptane = ((PhenoltoTridecene2 \times 0.167 + 0.0026 \times (1 - PhenoltoTridecene1$

469 $- PhenoltoTridecene2) \times 0.5) \times Phenol/94$

470 $+ 0.384 \times 0.1127 \times Aceticacid/60$

471 $+ 0.966 \times 0.25 \times Hydroxyacetone/74) \times 100$

472 $Tmcyclohexane$

473 $\quad = (0.0896 \times (1 - PhenoltoTridecene1$

474 $\quad - PhenoltoTridecene2) \times 0.6666 \times Phenol/94$

475 $\quad + 0.094 \times 0.6666 \times Dextrose/180 + 0.1987 \times (1 - PhenoltoTridecene1$

476 $\quad - PhenoltoTridecene2) \times 0.3333 \times Phenol/94 \times 2) \times 126$

477 $Pcyclohexane$

478 $\quad = (0.0896 \times (1 - PhenoltoTridecene1$

479 $\quad - PhenoltoTridecene2) \times 0.6666 \times Phenol/94$

480 $\quad + 0.094 \times 0.6666 \times Dextrose/180) \times 126$

481 $Pxylene = 0.0532 \times (1 - PhenoltoTridecene1$

482 $\quad - PhenoltoTridecene2) \times 0.75 \times Phenol/94 \times 106$

483 $Bicyclohexyl = (0.0052 \times (1 - PhenoltoTridecene1$

484 $\quad - PhenoltoTridecene2) \times 0.5 \times Phenol/94$

485 $\quad + 0.008 \times 0.5 \times Dextrose/180) \times 166$

486 $Xylenol = (0.0052 \times (1 - PhenoltoTridecene1$

487 $\quad - PhenoltoTridecene2) \times 0.75 \times Phenol/94$

488 $\quad + 0.376 \times 0.75 \times Dextrose/180) \times 122$

489 $Tmbenzene = (0.0026 \times (1 - PhenoltoTridecene1$

490 $\quad - PhenoltoTridecene2) \times 0.67 \times Phenol/94$

491 $\quad + 0.041 \times 0.5 \times Dextrose/180) \times 120$

492 $Cisdecalin = (0.036 \times 0.5 \times Dextrose/180 + 0.313 \times 0.5 \times Furfural/96) \times 138$

493 $Bcyclohexane = (0.012 \times 0.5 \times Dextrose/180 + 0.005 \times 0.5 \times Furfural/96) \times 140$

494 $Tmheptane = (0.232 \times 0.5 \times Furfural/96) \times 142$

495 $Dmebenzene = (0.204 \times 0.5 \times Furfural/96) \times 134$

496     $Mcyclohexane$

497     $= (PhenoltoTridecene2 \times 0.167 + 0.1351 \times (1 - PhenoltoTridecene1$

498     $- PhenoltoTridecene2) \times 0.3344) \times Phenol \times 2/94 \times 0.9 \times 98$

499     $Thnaphthalene = Mcyclohexane \times 0.07483$

500     $JetFuel = Tridecene + Diamantane + Diphenyl + Triethylbenezene + Heptane$

501     $+ Tmcyclohexane + Pcyclohexane + Pxylene + Bicyclohexyl$

502     $+ Xylenol + Tmbenzene + Cisdecalin + Bcyclohexane + Tmheptane$

503     $+ Dmebenzene + Mcyclohexane + Thnaphthalene$

504     $HydrogenNeeded$

505     $= (PhenoltoTridecene1 \times 4 + PhenoltoTridecene2 \times 2.83$

506     $+ (0.1766 \times 2.29 + 0.1390 \times 0.5 + 0.1351 \times 1.33 + 0.0961 \times 2.5$

507     $+ 0.0896 \times 4 \times 2 + 0.0532 \times 1.75 + 0.0065 \times 3.33 + 0.0052 \times 3.5$

508     $+ 0.0052 + 0.0026 \times 2 + 0.0026 \times 5.5) \times (1 - PhenoltoTridecene1$

509     $- PhenoltoTridecene2)) \times Phenol/94 \times 2 + (3 \times 0.376 + 0.67 \times 0.196$

510     $+ 8 \times 0.124 + 6 \times 0.094 + 6 \times 0.094 + 2 \times 0.041 + 4.5 \times 0.036$

511     $+ 2.33 \times 0.02 + 5 \times 0.012 + 5.5 \times 0.008) \times Dextrose/180 \times 2$

512     $+ (4.5 \times 0.313 + 5.5 \times 0.232 + 3.5 \times 0.204 + 10 \times 0.139 + 4 \times 0.108$

513     $+ 5 \times 0.005) \times Furfural/96 \times 2 + (1.5 \times 0.616$

514     $+ 2.22 \times 0.384) \times Aceticacid/60 \times 2 + (2 \times 0.966$

515     $+ 5 \times 0.034) \times Hydroxyacetone/74 \times 2 + (1.75 \times 0.954$

516     $+ 0.046) \times Formicacid/46 \times 2 + Mcyclohexane/98 \times 9 \times 2$

517     $+ 0.1987 \times (1 - PhenoltoTridecene1$

518     $- PhenoltoTridecene2) \times 0.3333 \times Phenol/94 \times 12 \times 2$

$AlkanestoReforming$

$$= 0.1351 \times 0.33 \times (1 - PhenoltoTridecene1$$

$$- PhenoltoTridecene2) \times Phenol/94 \times 58$$

$$+ PhenoltoTridecene2 \times 0.167 \times Phenol/94 \times 30 + 0.0065 \times 0.33 \times (1$$

$$- PhenoltoTridecene1 - PhenoltoTridecene2) \times Phenol/94 \times 58$$

$$+ 0.0026 \times 0.5 \times (1 - PhenoltoTridecene1$$

$$- PhenoltoTridecene2) \times Phenol/94 \times 58 + 0.0026 \times 0.5 \times (1$$

$$- PhenoltoTridecene1 - PhenoltoTridecene2) \times Phenol/94 \times 16$$

$$+ (0.124 \times 5 + 0.041 \times 0.5 + 0.036 \times 0.5 + 0.02 \times 0.33$$

$$+ 0.012 \times 0.5) \times Dextrose/180 \times 16 + (5 \times 0.139$$

$$+ 0.108) \times Furfural/96 \times 16 + 0.108 \times Furfural/96 \times 44 + ((0.5 \times 30$$

$$+ 0.5 \times 16) \times 0.616 + (58 + 44 + 30$$

$$+ 16) \times 0.11 \times 0.384) \times Aceticacid/60 + ((44 + 16) \times 0.25 \times 0.966$$

$$+ 3 \times 16 \times 0.034) \times Hydroxyacetone/74 + ((30 + 16) \times 0.25 \times 0.954$$

$$+ 16 \times 0.5 \times 0.046) \times Formicacid/46$$

$$+ Mcyclohexane/98/0.9 \times 0.1 \times 58/2$$
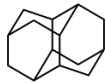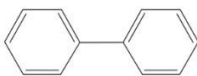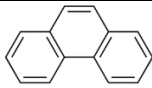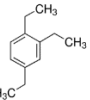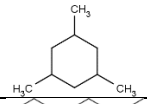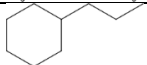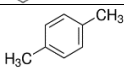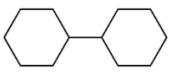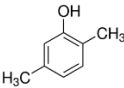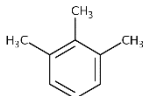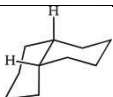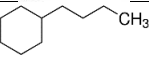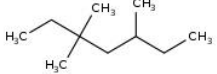
$$
\begin{aligned}
SteamProduced \\
&= (PhenoltoTridecene1 + PhenoltoTridecene2 + (0.1987 + 0.1766 \\
&\quad + 0.1390 + 0.1351 + 0.0961 + 0.0896 \times 2 + 0.0532 + 0.0065 \times 0.33 \\
&\quad + 0.0052 + 0.0052 \times 0.25 + 0.0026 + 0.0026) \times (1 \\
&\quad - PhenoltoTridecene1 - PhenoltoTridecene2)) \times Phenol\,/\,94 \times 18 \\
&\quad + (5.25 \times 0.376 + 3.33 \times 0.196 + 4 \times 0.124 + 6 \times 0.094 + 6 \times 0.094 \\
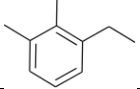&\quad + 4 \times 0.041 + 5 \times 0.036 + 3.33 \times 0.02 + 5 \times 0.012 \\
&\quad + 6 \times 0.008) \times Dextrose\,/\,180 \times 18\ +\ (2 \times 0.313 + 2 \times 0.232 \\
&\quad + 2 \times 0.204 + 2 \times 0.139 + 2 \times 0.005) \times Furfural\,/\,96 \times 18\ +\ (0.616 \\
&\quad + 1.78 \times 0.384) \times Aceticacid\,/\,60\ \times 18\ +\ (1.5 \times 0.966 \\
&\quad + 2 \times 0.034) \times Hydroxyacetone\,/\,74\ \times 18\ +\ (1.5 \times 0.954 \\
&\quad + 0.046) \times Formicacid\,/\,46\ \times 18
\end{aligned}
$$

Equation 6

Renewable jet fuel property correlations from its constituent chemical compositions are first time developed in this research that can help to comply with the ASTM D7566 standard. Table 2 shows the renewable jet fuel components. Their properties extracted from Aspen Plus 8.8 are shown in Table 2. These properties are specific gravity, cetane number, aniline point, flash point and volumetric average boiling point (VABP). In addition, % mass of hydrogen and % volume of aromatics are also required for the ASTM D7566 standard, which can be estimated from the total amount of hydrogen present in all the renewable jet fuel chemical constituents and the total amount of aromatics present in the renewable jet fuel (diamantane, diphenyl, 1,2,4-triethylbenzene, p-xylene, 2,5-xylenol, 1,2,3-trimethylbenzene and 1,2-dimethyl-3-ethylbenzene).

558   Table 2. Properties of renewable jet fuel chemical constituents for the ASTM D7566 standard.

Renewable jet fuel chemical constituents	Structure	Molar mass	Specific gravity	Cetane number	Aniline point ^{o}C	Flash point ^{o}C	Volumetric average boiling point (VABP) ^{o}C
1-tridecene		182	754	76	86	91	233
diamantane		188	1033	13	-75	103	256
diphenyl		154	1029	14	-65	103	255
phenanthrene		178	1137	13	-51	138	337
1,2,4-triethylbenzene		162	873	28	28	82	218
n-heptane		100	682	33	70	-5	99
1-*trans*-3,5-trimethylcyclohexane		126	775	31	44	28	141
n-propylcyclohexane		126	790	31	40	41	157
p-xylene		106	861	19	-25	27	139
bicyclohexyl		166	883	28	32	94	239
2,5-xylenol		122	1008	14	-78	78	211
1,2,3-trimethylbenzene		120	894	20	-20	54	176

cis-decalin		138	894	21	-8	68	196
n-butylcyclohexane		140	795	37	51	58	181
3,3,5-trimethylheptane		142	739	44	68	40	156
1,2-dimethyl-3-ethylbenzene		134	888	22	-4	66	194
methylcyclohexane		98	766	22	15	-3	101
1,2,3,4-tetrahydronaphthalene		132	972	15	-53	75	208

559

560

27

561   Empirical correlations in Equation 7 are derived by linear regression, for the renewable jet fuel

562   product properties from its individual chemical constituent properties. The overall renewable

563   jet fuel and its constituent chemical properties are extracted from Aspen Plus 8.8. Equation 7

564   gives an important checkpoint for meeting the specified range of specific gravity, minimum

565   cetane number, aniline point, flash point and % mass of hydrogen and maximum VABP and %

566   volume of aromatics for the renewable jet fuel product.

567   *Specific gravity*

$$568 \quad = \frac{\sum((Specific\ gravity\ of\ constituent) \times (Number\ of\ moles\ of\ constituent))}{Number\ of\ moles\ of\ bio\ jet\ fuel\ product}$$

569   *Cetane number*

$$570 \quad = \frac{\sum((Cetane\ number\ of\ constituent)^{1.04} \times (Number\ of\ moles\ of\ constituent))}{Number\ of\ moles\ of\ bio\ jet\ fuel\ product}$$

571   *Aniline point* (K)

$$572 \quad = \frac{\sum((Aniline\ point\ of\ constituent + 273)^{1.011} \times (Number\ of\ moles\ of\ constituent))}{Number\ of\ moles\ of\ bio\ jet\ fuel\ product}$$

573   *Flash point* (K)

$$574 \quad = \frac{\sum((Flash\ point\ of\ constituent + 273) \times (Number\ of\ moles\ of\ constituent))}{Number\ of\ moles\ of\ bio\ jet\ fuel\ product}$$

$$575 \quad VABP\ (^oC) = \frac{\sum((VABP\ of\ constituent) \times (Number\ of\ moles\ of\ constituent))}{Number\ of\ moles\ of\ bio\ jet\ fuel\ product}$$

576   Equation 7

577   Mass and energy balance around steam reforming, PSA, CHP and MIEC

578   Alkanes are produced from flash columns of the reboiler distillation train (Fig. 1). The previous

579   publication discusses the integrated bio-oil hydrodeoxygenation, decanter, reboiler distillation

580   (without condensers) train with flash columns and hydrocracking process, alongside its Aspen

581   Plus simulation, to produce gasoline and green diesel (Sadhukhan and Ng, 2011). Appendix A

582   gives an overview of the previous findings to complement the mathematical models for the

583   design evaluations of the integrated self-sustainable biorefinery system. This is to enable the

584   biorefinery system evaluations without the use of proprietary process simulation packages,

585   Aspen Plus® (Sadhukhan and Ng, 2011) and Superpro Designer® (Martinez-Hernandez et al.,

586   2019).

587   Steam reforming of alkanes is highly endothermic completed at and above 750°C and at 15-25

588   bar pressure (Kolios et al., 2005). Equation 8 is a generic form of steam reforming reaction of

589   alkanes.

590    $C_nH_m + nH_2O \rightarrow nCO + (0.5m + n)H_2$ Equation 8

591   From the known quantities of alkanes ($AlkanestoReforming$ in Equation 6), the amounts of

592   steam needed and hydrogen and CO produced are determined based on the reaction

593   stoichiometry in Equation 8. Equation 9 shows these mass balances.

594 $HydrogenfromReforming$

595 $= 0.1351 \times 0.33 \times (1 - PhenoltoTridecene1$

596 $- PhenoltoTridecene2) \times Phenol \, / \, 94 \times 9 \times 2$

597 $+ PhenoltoTridecene2 \times 0.167 \times Phenol \, / \, 94 \times 5 \times 2$

598 $+ 0.0065 \times 0.33 \times (1 - PhenoltoTridecene1$

599 $- PhenoltoTridecene2) \times Phenol \, / \, 94 \times 9 \times 2 + 0.0026 \times 0.5 \times (1$

600 $- PhenoltoTridecene1 - PhenoltoTridecene2) \times Phenol \, / \, 94 \times 9 \times 2$

601 $+ 0.0026 \times 0.5 \times (1 - PhenoltoTridecene1$

602 $- PhenoltoTridecene2) \times Phenol \, / \, 94 \times 3 \times 2 + (0.124 \times 5$

603 $+ 0.041 \times 0.5 + 0.036 \times 0.5 + 0.02 \times 0.33$

604 $+ 0.012 \times 0.5) \times Dextrose \, / \, 180 \times 3 \times 2 + (5 \times 0.139$

605 $+ 0.108) \times Furfural \, / \, 96 \times 3 \times 2 + 0.108 \times Furfural \, / \, 96 \times 7 \times 2$

606 $+ ((0.5 \times 5 \times 2 + 0.5 \times 3 \times 2) \times 0.616 + (9 + 7 + 5$

607 $+ 3) \times 2 \times 0.11 \times 0.384) \times Aceticacid \, / \, 60 + ((7$

608 $+ 3) \times 2 \times 0.25 \times 0.966 + 3 \times 3 \times 2 \times 0.034) \times Hydroxyacetone \, / \, 74$

609 $+ ((5 + 3) \times 2 \times 0.25 \times 0.954$

610 $+ 3 \times 2 \times 0.5 \times 0.046) \times Formicacid \, / \, 46$

611 $+ Mcyclohexane \, / \, 98 \, / 0.9 \times 0.1 \times 9$

$SteamneededReforming$

$$= 0.1351 \times 0.33 \times (1 - PhenoltoTridecene1$$

$$- PhenoltoTridecene2) \times Phenol\ /\ 94 \times 4 \times 18$$

$$+ PhenoltoTridecene2 \times 0.167 \times Phenol\ /\ 94 \times 2 \times 18$$

$$+ 0.0065 \times 0.33 \times (1 - PhenoltoTridecene1$$

$$- PhenoltoTridecene2) \times Phenol\ /\ 94 \times 4 \times 18 + 0.0026 \times 0.5 \times (1$$

$$- PhenoltoTridecene1$$

$$- PhenoltoTridecene2) \times Phenol\ /\ 94 \times 4 \times 18 + 0.0026 \times 0.5 \times (1$$

$$- PhenoltoTridecene1 - PhenoltoTridecene2) \times Phenol\ /\ 94 \times 18$$

$$+ (0.124 \times 5 + 0.041 \times 0.5 + 0.036 \times 0.5 + 0.02 \times 0.33$$

$$+ 0.012 \times 0.5) \times Dextrose\ /\ 180 \times 18 + (5 \times 0.139$$

$$+ 0.108) \times Furfural\ /\ 96 \times 18 + 0.108 \times Furfural\ /\ 96 \times 3 \times 18$$

$$+ ((0.5 \times 2 + 0.5) \times 18 \times 0.616 + (4 + 3 + 2$$

$$+ 1) \times 18 \times 0.11 \times 0.384) \times Aceticacid\ /\ 60 + ((3$$

$$+ 1) \times 18 \times 0.25 \times 0.966 + 3 \times 18 \times 0.034) \times Hydroxyacetone\ /\ 74$$

$$+ ((2 + 1) \times 18 \times 0.25 \times 0.954 + 18 \times 0.5 \times 0.046) \times Formicacid\ /\ 46$$

$COtoCHP = AlkanestoReforming - HydrogenfromReforming$

$$+ SteamneededReforming$$

Equation 9

The alkane steam reforming produces a gas mixture containing hydrogen and carbon monoxide. A PSA can separate hydrogen from the CO-rich offgas (Riboldi and Bolland, 2016). PSA has been investigated for ultrapure hydrogen production in an integrated gasification combined cycle system (Riboldi and Bolland, 2016). The CO-rich offgas is routed to CHP along with the pyrolysis gas. The produced and purified hydrogen from alkane steam reforming and PSA is added to the stream of hydrogen from MIEC discussed later.

637 Carbon monoxide and pyrolysis gas have a heat of combustion of 10 and 23 MJ per kg,

638 respectively, which form the basis for the CHP modelling (Sadhukhan et al., 2021). The heat

639 output from the gas boiler is 80% of the heat of combustion of the CHP fuel. The medium

640 pressure steam separated from the stable bio-oil in the decanter and generated by the indirect

641 heat recovery from exothermic heat of hydroprocessing reactions can be turned into high

642 pressure superheated steam, in the gas boiler in the CHP. Most of the high pressure superheated

643 steam from the CHP is used in alkane steam reforming and MIEC, to produce hydrogen. The

644 latter also produces oxygen for the CHP. Some steam generated by heat recovery in the gas

645 boiler can be expanded through a back pressure steam turbine to generate electricity for the

646 biorefinery use, biomass drying and size reduction (pretreatment of biomass before pyrolysis)

647 and to drive the flows across the biorefinery. The remaining medium pressure steam from the

648 site can be exported.

649 Electrochemical technologies such as MIEC offer energy efficiency and flexibility across the

650 scale, and process intensification opportunities deploying nature-based chemical engineering

651 solutions (Thursfield and Metcalfe, 2004; Trogadas and Coppens, 2020). However, the use of

652 MIEC is more popularly known for oxygen reduction reaction (ORR) applied to

653 electrochemical systems for energy storage and generation. MIEC can also be used for steam

654 splitting or air separation. Amongst the various types of MIEC, perovskite and its derivatives

655 have been proven to be most effective (Raja et al., 2017). Since perovskites' discovery in 1839

656 by Gustav Rose and naming by LA Perovski, perovskites (ABO_3, $A_{n+1}B_nO_{3n+1}$, $AA'B_2O_6$ and

657 $A_2BB'O_6$) have been researched extensively for structural, electronic and surface

658 characteristics and mechanisms of oxygen ion transport (Ji et al., 2020). Amongst the various

659 mechanistic hypotheses, the most popular mechanism driving the ORR shows the B-site cations

660 of perovskites participating in the redox reactions and the A-site cations of perovskites offering

661 large ionic radii, thus favourable crystal and electronic structure for ionic activity. The

32

662 transition metals with incomplete 3d orbitals are the ideal candidates for the B-site cations,

663 while the alkaline earth metals and lanthanides are the choices for the A-site cations of

664 perovskites, such as, in the following order of preference in decreasing order of ionic radius:

665 La > Pr > Nd > Sm > Gd > Y > Dy > Yb (Geffroy et al., 2013; Risch, 2017). Mn, Fe, Co and

666 Ni are examples of B-site cations and La and Sr for A-site cations. Twelve and six oxygen

667 anions attach to the A-site and B-site cations in an example study on a cubic perovskite oxide.

668 There is already a handful of dedicated research on MIEC for hydrogen and oxygen

669 productions (Li et al., 2017; Arratibel Plazaola et al., 2019), as shown above. However, none

670 of them has considered MIEC in the context of hydroprocessing technologies. Inspired by

671 existing studies, this research conducts mass and energy balances based on ideal splits around

672 the MIEC and various interacting unit processes. MIEC is used to meet the balance of the

673 hydrogen requirements by the hydrodeoxygenation and hydrocracking reactions. Their

674 hydrogen demands are first met by steam reforming of the alkanes produced from flash

675 columns in the reboiler distillation train attached to hydrodeoxygenation and hydrocracking

676 reactors and the decanter. Then, the rest of the hydrogen demands is met by the MIEC. The

677 mass balances around the MIEC and CHP are shown in Equation 10.

678 $HydrogenfromSteam = HydrogenNeeded - HydrogenfromReforming$

679 $OxygenfromSteam = (HydrogenfromSteam)/2 \times 16$

680 $MIECFeed = HydrogenfromSteam + OxygenfromSteam$

681 $ExcessSteam = SteamProduced + Water - HydrogenfromSteam -$

682 $OxygenfromSteam - SteamneededReforming$

683   Equation 10

Economic value and an overall sustainability assessment

685 The economic value analysis involves estimations of the delivered cost of equipment, total

686 capital cost, operating cost, feedstock cost and product values. The revenues are generated from

687   selling the marketable products. Furthermore, any credits on products are added to the

688   revenues. Taxations, and landfill and emission charges are subtracted from the revenues. A

689   value analysis methodology has been developed to compute value on processing and cost of

690   production (COP) of various streams in a system (Martinez-Hernandez et al., 2013; Martinez-

691   Hernandez et al., 2014). The COP calculation method is applied for the final products from the

692   biorefinery system.

693   The evaluation of COP of a stream starts from the known market price of feedstocks, added

694   with the costs incurred from its production, thus proceeds in the forward direction until end

695   products' evaluations. The COP of a stream is the summation of all associated cost components

696   (i.e. the costs of feedstocks, utilities, operating (including personnel) and annualised capital

697   costs) that have contributed to the production of that stream up to that point. This must mean

698   the inclusion of only those fractional costs involved with the stream's production. To compute

699   COP, the annual capital and operating costs are computed as follows.

700   For the annual capital cost, the total capital and delivered cost of equipment are estimated. The

701   delivered cost of equipment is estimated using the well know size-cost correlation in Equation

702   11 that captures the economy of scale and monetary depreciation (Sadhukhan et al., 2014;

703   Sadhukhan et al., 2021).

704      $NEW\ COST\ AT\ THE\ BASE\ YEAR = BASE\ COST \times \left(\frac{NEW\ SIZE}{BASE\ SIZE}\right)^{SCALE\ FACTOR}$

705      $NEW\ COST\ AT\ THE\ CURRENT\ YEAR = NEW\ COST\ AT\ THE\ BASE\ YEAR \times$

706      $\frac{CEPCI\ AT\ THE\ CURRENT\ YEAR}{CEPCI\ AT\ THE\ BASE\ YEAR}$ Equation 11

707      $CEPCI$ is the Chemical Engineering Plant Cost Index. The $CEPCI$ stabilised at 600 in recent

708   years has been applied to update the $NEW\ COST\ AT\ THE\ CURRENT\ YEAR$.

709   Table 3 shows the input data for the calculation of the delivered cost of equipment of the

710   system. The data comprise a given size-cost data and a scale factor for each unit process in the

711 system, pyrolysis, hydrodeoxygenation and hydrocracking, distillation and decanter, PSA,

712 MIEC, steam reforming and CHP, compiled from Sadhukhan et al. (2014).

713 Table 3. Size-cost correlation data for the calculation of the delivered cost of equipment

714 (Sadhukhan et al., 2014).

	base cost m$	scale factor	base size	unit	CEPCI
Pyrolysis	3.392	0.7	500	tpd biomass	402
Hydrodeoxygenation and hydrocracking	30	0.65	2250	bblpd bio-oil	468.2
Distillation and decanter	2.28	0.65	2250	bblpd bio-oil	525.4
PSA	28	0.7	9600	kmolph gas input	394.3
MIEC	21.6	0.8	17	tph H_2 recovered	394.3
Steam reforming	9.4	0.6	1390	kmolph gas input	394.3
CHP	5.1	0.7	10.3	MWe electricity output	394.3

715

716 The total capital cost can be up to 5.03 times the delivered cost of equipment for a solid-fluid

717 processing system to account for the various capital costs outside the battery limit (Sadhukhan

718 et al. 2014). An annual capital charge of 0.13 has been applied for the annual capital cost

719 (Sadhukhan et al., 2014).

720 In addition, annual operating cost and feedstock cost need to be considered for the total cost of

721 production of the system. The annual operating cost ($Opex$) consists of fixed and variable (raw

722 materials and utilities, etc.) costs. The operating cost estimation has a generic form as in

723 Equation 12.

724 $Opex = a \times (fixed\ operating\ cost\ dependent\ on\ indirect\ annual\ capital\ cost +$

725 $labour\ dependent\ fixed\ operating\ cost\ +\ variable\ operating\ cost)$

726

727   *fixed operating cost dependent on indirect annual capital cost*

728               $= b \times Delivered\ cost\ of\ equipment \times Annual\ Capital\ Charge$

729   *labour dependent fixed operating cost* $= c \times Feedstock\ throughput$

730   Equation 12

731 a, b and c are multipliers of the respective cost components to account for a sub-set of cost

732 components detailed in Sadhukhan et al. (2014). Fixed operating costs include the costs of

733 maintenance, labour, taxation, insurance, royalties etc. Fixed operating costs are estimated

734 using factors, normally based on indirect capital cost and labour cost. Other than the fixed and

735 variable operating costs, there are costs of research and development, sales expenses and

736 general overheads accounted for as % to obtain the total operating cost. The value of a in

737 Equation 12 is 1.3 (Sadhukhan et al., 2021).

738 The indirect capital cost is 1.26 times the delivered cost of equipment for a solid-fluid

739 processing system (Sadhukhan et al., 2014). The indirect capital cost includes the following

740 cost items: engineering and supervision, construction expenses, legal expenses, contractor's

741 fee and contingency. Furthermore, the fixed operating cost dependent on the indirect capital

742 cost is 0.15 times the indirect capital cost. The fixed operating cost dependent on the indirect

743 capital cost includes the following cost items: maintenance, capital charges, insurance, local

744 taxes and royalties. The value of b in Equation 12 is $1.26 \times 0.15 = 0.19$.

745 The fixed operating cost dependent on the personnel cost is 1.9 times the personnel cost. The

746 fixed operating cost dependent on the personnel cost includes the following cost items: labour,

747 laboratory, supervision and plant overheads. The personnel cost is \$52033 per t/h throughput.

748 Thus, the value of c in Equation 12 is $1.9 \times 52033/1000000 = 0.1$. For detailed correlations

749 and breakup of cost items, readers are directed to Chapter 2 in Sadhukhan et al. (2014).

750 For the brevity of this paper, LCA methodologies are not discussed here (see Sadhukhan et al.,

751 2014 for the LCA methodology). In this research, two primary life cycle impact potentials,

global warming, and fossil resource depletion potentials are estimated by applying the factors from published literature. It has been established that 10 g CO_2 equivalent per MJ for well-to-wake systems utilising non-food cellulosic biomass is the best greenhouse gas emissions outcome, in renewable jet fuel production (Kolosz et al., 2020). The conventional and renewable jet fuels have the global warming potentials of 83.3 and 10 g CO_2 equivalent per MJ, respectively, thus giving a saving of (83.3-10) or 73.3 g CO_2 equivalent of global warming potential by the displacement of 1 MJ worth of conventional jet fuel by the renewable jet fuel (EU RED, 2018). 40 MJ/kg primary energy saving can be applied for this displacement (EU RED, 2018).

The SLCA must also be conducted to avoid unintended consequences on society (Sadhukhan et al., 2021). The SLCA has now become more practicable with the emergence of the social hotspot database (SHDB) (Benoît et al., 2010; Norris et al., 2014). In the SHDB, for each country, inventory data (in terms of monetary value) has been assimilated for each product type or sector. As inevitable, each product type or sector is dependent on every other product type or sector. The inventory data for each product type or sector for each country through interconnecting supply chains is translated into social life cycle impact assessments, in five main categories: labour rights & decent work; health & safety; human rights; governance; and community infrastructure (Shemfe et al., 2018). The supply chain import-export data between countries considering interacting supply chains can be assimilated from the UN Comtrade database (Sadhukhan et al., 2019; Sadhukhan et al., 2021). The present SHDB platform allows comparisons of medium-risk hours-equivalent (mrh eq.) for a given product between countries of interest in each category. The unit of risks is mrh for a given functional unit, e.g. rate of product formation in case of a production system. The unit mrh is the number of work hours applied to produce a given production rate. In here, a dimensionless ratio between mrh in business-as-usual import case and mrh in self-generation case for a given production rate is

777 considered for each of the SLCA impact categories to show the benefits or savings by

778 indigenous energy security services in social and socio-economic quantitative terms,

779 recommended by the ISO26000 (Sadhukhan et al., 2019; Sadhukhan et al, 2021).

780 **Results and discussions**

781 The biorefinery system's design, techno-economic and sustainability analyses model is

782 implemented through an interactive graphical user interface friendly open source platform:

783 TESARREC™, https://tesarrec.web.app/sustainability/bio-jet-fuel (TESARREC™, 2018 and

784 2020). The computing code, including for Equations 3-4, 6-7, 9-10, and 11-12, for the

785 TESARREC™, https://tesarrec.web.app/sustainability/bio-jet-fuel (TESARREC™, 2018 and

786 2020) simulation model can be accessed in Sen (2020). Here, specific insights into the results

787 of the mathematical model for the integrated biorefinery system under consideration are

788 discussed.

789 Table 4 shows the input variables for the biorefinery system's design, techno-economic and

790 sustainability evaluations. Regarding mass and energy balance calculations, the input variables

791 are bio-oil mass throughput and composition, biomass calorific values, and fractional

792 conversion of an important bio-oil constituent, phenol, in Reactions 1 and 7 in Equation 5.

793 Table 4 shows their ranges as well as default values. In the TESARREC™ platform,

794 https://tesarrec.web.app/sustainability/bio-jet-fuel, all the input variables can be varied within

795 the ranges shown in Table 4 to test their sensitivity on the outputs. Here, the results

796 corresponding to the default values are shown. The ranges shown in Table 4 define the

797 conditions under which the biorefinery design and models are very suitable to use. While the

798 biorefinery design is generic, the stoichiometric chemical reaction model of hydroprocessing

799 can be updated for a different set of bio-oil chemical constituents and hydroprocessing

800 reactions using the generic modelling principles presented in this paper.

801 Table 4. Input variables for the renewable jet fuel-producing biorefinery system model.

	Default value	Range
Bio-oil throughput kg/hour	10000	10000-50000
Phenol in bio-oil (fraction)	0.33	0.31-0.38
Dextrose in bio-oil (fraction)	0.27	0.27-0.30
Furfural in bio-oil (fraction)	0.077	0.07-0.10
Acetic acid in bio-oil (fraction)	0.056	0.05-0.06
Hydroxyacetone in bio-oil (fraction)	0.04	0.04-0.05
Formic acid in bio-oil (fraction)	0.015	0.01-0.015
Water in bio-oil (fraction)	0.212	0.10-0.25
Biomass calorific value MJ/kg	19.3	13-23
Phenol fractional conversion in Reaction 1 in Equation 5	0.55	0.158-0.55
Phenol fractional conversion in Reaction 7 in Equation 5	0.4	0.072-0.4
Installation factor	1	1-5
Annual capital charge	0.13	0.1-0.15
Biomass cost $/t	40	10-100
Jet fuel price $/gallon	1	1-2
Char price $/t	100	100-600
Steam price $/t	24.4	24.4-35.5

802

803 For the default values of input variables, as shown in Table 4, the flowrates of the various outlet

804 streams within and between the various process units are determined, as shown in Fig. 4. The

805 input variables for technical modelling of the systems are bio-oil throughput and composition,

806 and phenol conversions in Reactions 1 and 7 in Equation 5. A higher concentration of 1-

807 tridecene in renewable jet fuel enhances the properties of renewable jet fuel. The technical

808 outputs are determined from the input variables as follows. Biomass throughput, and pyrolysis

809 gas and char yields are calculated for a given bio-oil mass flowrate, under fast pyrolysis and

810 500°C temperature conditions, using Equations 3-4. The mass balance Equation 6 is used to

811 determine the renewable jet fuel amount and concentrations. Renewable jet fuel is made up of

812 higher hydrocarbons (>C7) produced by the reactions shown in Equation 5. Similarly, the

813 amount and concentrations of alkanes for steam reforming are determined using Equation 6.

814 The mass balance in Equation 9 is used to estimate the amounts of hydrogen and CO produced

815 and steam used in alkane reforming. Thus, the amount of CHP fuel is estimated from the

816 amounts of pyrolysis gas (Equations 3-4) and carbon monoxide (Equation 9). The total

817   hydrogen consumption is estimated from the reaction balance equations in Equation 6. The

818   balance between hydrogen consumption and hydrogen production by alkane steam reforming

819   decides the amounts of hydrogen and oxygen produced and steam used by MIEC (Equation

820   10). The other input variables shown in Table 4 are discussed later in the context of the

821   economic value analysis of the biorefinery system.

822
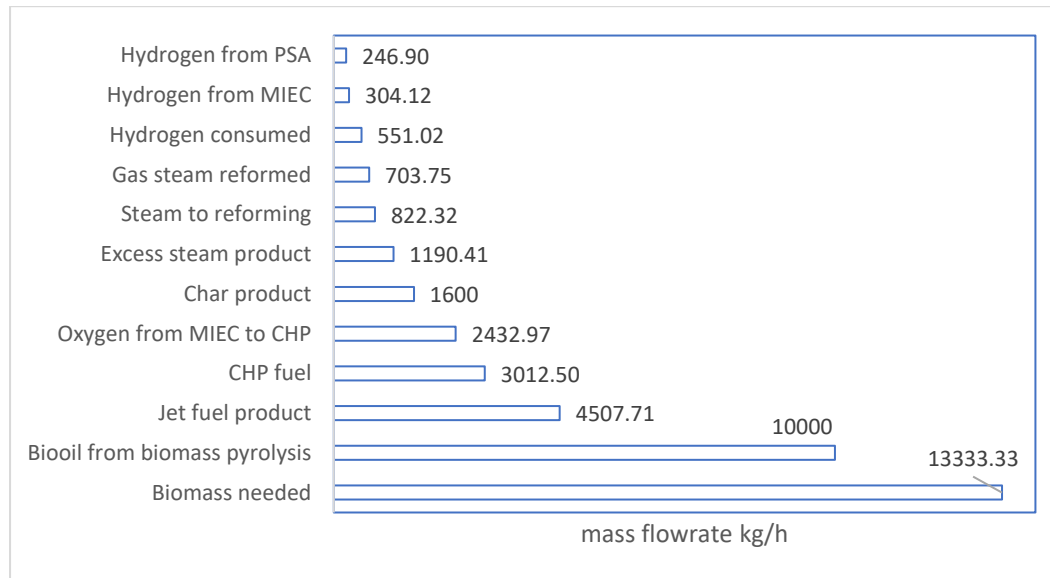
823   **Fig. 4** Mass flowrates (kg/h) in the biorefinery system configuration in Fig. 1 for the default

824   input variable values in Table 4.

825   Fig. 4 shows the production rates based on the default values in Table 4. The production rate

826   of renewable jet fuel from the biorefinery system is 34% by mass of biomass. The fast pyrolysis

827   process gives pyrolysis gas, bio-oil and char yields of 13%, 75% and 12% of the mass of

828   biomass (Equations 3-4, Fig. 3). Hydrogen consumed in bio-oil hydrodeoxygenation and

829   hydrocracking is 5.5% by mass of bio-oil (Equation 6). Alkanes produced from distillation,

830   which are steam reformed, are 7% by mass of bio-oil (Equation 6). Hydrogen produced from

831   steam reforming is 2.5% by mass of bio-oil (Equation 9). Thus, the balance of hydrogen

832   produced from MIEC is 3% by mass of bio-oil (Equation 10). Oxygen produced from MIEC

833   is thus 24% by mass of bio-oil (Equation 10). Fuel to CHP (pyrolysis gas plus PSA offgas) is

834   30% by mass of bio-oil. Note the transferability of these production rates in other studies for

835   known bio-oil throughput and composition.

836   Pyrolysis reactors can be of various types, bubbling fluidised bed, circulating fluidised bed,

837   ablative, auger/screw, rotating cone, and vacuum (Sadhukhan et al., 2014). Amongst these, a

838   circulating fluidised bed can offer a vapour residence time of 0.5-1s, an operating temperature

839   of 500°C, high heat transfer rate, large throughput, robust temperature control, and good

840   mixing, required for the fast pyrolysis reaction in the biorefinery system. A rotating cone can

841   form the bottom of the pyrolyser reactor to remove solid to avoid any solid build-up.

842   Hydroprocessing as mentioned earlier is made up of two reactors, hydrodeoxygenation (150-

843   250°C) and hydrocracking (350-400°C). These reactions are exothermic. Their exothermic heat

844   of reactions can be recovered into the generation of medium pressure steam through cooling

845   jackets surrounding the reactors. These reactions are driven by high hydrogen pressure, 80-170

846   bar. Excess hydrogen can be kept in circulation around the system. Only the hydrogen

847   consumed in the reactions in Equation 5 is needed to be produced within the system.

848   Fig. 5 shows the energy balance analysis of the integrated biorefinery system configuration.

849   The thickness of each arrow is proportional to its relative energy content for other flows.
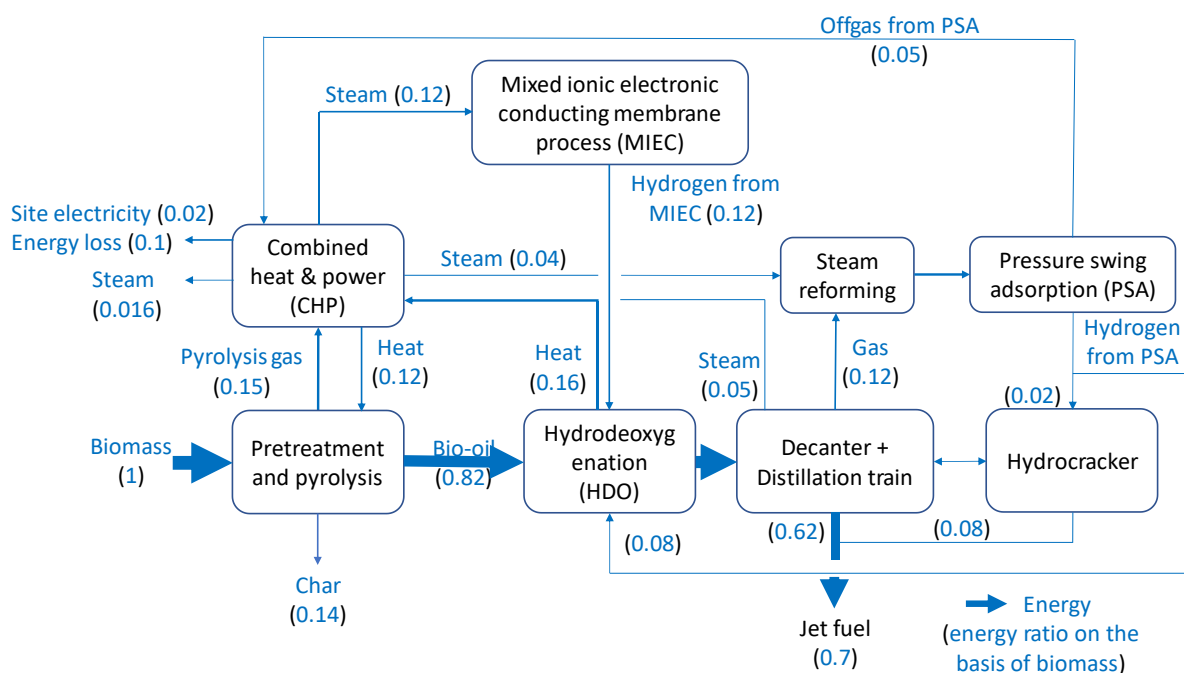
Fig. 5 Energy flows (as the ratio between energy content in each flow and energy content in biomass) exchanged between the various unit processes and from the biorefinery system.

The energy flows relative to the biomass energy flow are shown in Fig. 5. The basis of energy flow calculations is 1 unit of energy flow in biomass. Biomass throughput and calorific value can be applied to upscale the energy flows shown in Fig. 5. Pretreatment and pyrolysis of biomass have the energy inputs through the biomass (1) and medium grade heat from CHP (0.12). The energy outputs from the pyrolysis are through the pyrolysis gas (0.15), bio-oil (0.82) and char (0.14). These outlet streams are estimated to have a calorific value of 23, 21.08 and 23 MJ/kg, respectively. Hydrodeoxygenation takes up hydrogen from MIEC (0.12) and hydrogen from PSA (0.08) and is a source of medium grade steam (0.16). The balance of its energy output (bio-oil energy (0.82) plus hydrogen energy (0.2) input subtracted by the medium grade heat recovered (0.16)), is equal to the energy input to the decanter and distillation train (0.86). The outputs from decanter and distillation are renewable jet fuel (0.62), gas to reformer (0.12) and decanted steam (moisture contained in bio-oil, and steam produced according to the balance Equation 6) (0.05). Renewable jet fuel has a calorific value of 40 MJ/kg. The medium

grade heat or steam recovered from hydrodeoxygenation, decanter and distillation train, is

upgraded into high pressure superheated steam generation at 750°C for reforming (0.04) and

MIEC (0.12) in the gas boiler in CHP. The reforming hydrogen production capacity and thus,

its heat demand, is constrained by the gas availability from the distillation train. The balance

of the hydrogen demands by hydrodeoxygenation and hydrocracking is met by MIEC that

utilises high pressure superheated steam. The biorefinery system is a net source of heat or

steam. Hydrogen energy from steam reforming and MIEC is 0.1 and 0.12, respectively. The

CHP fuels are the pyrolysis gas (0.15) and PSA offgas (0.05). After upgrading medium pressure

steam into high pressure superheated steam (0.16), and meeting pretreatment and pyrolysis heat

demand (0.12), the balance of energy from CHP goes into the following, energy loss (0.1) due

to efficiency loss in the boiler (operates at 80% energy efficiency) and in back pressure steam

turbine expanding high pressure superheated steam into electricity generation (operates at 28%

energy efficiency), electricity to meet site demand (0.02), and excess medium pressure steam

to export (0.016). The energy outputs from the biorefinery system relative to the biomass

energy input are through the renewable jet fuel product (0.7), char (0.14) and excess medium

pressure steam (0.016), thus resulting in an overall biorefinery energy efficiency of 85.6%.

The renewable jet fuel property correlations from its constituent chemical compositions in

Equation 7 are applied to determine the overall properties of the renewable jet fuel product.

The amounts of the renewable jet fuel chemical constituents are adjusted to meet the ASTM

D7566 standards for the specific gravity, cetane number, aniline point, flash point, VABP, %

mass hydrogen and % volume aromatics of the renewable jet fuel product. Equation 6 shows

the calculations for the renewable jet fuel and its chemical constituent amounts. Table 5 shows

the overall renewable jet fuel properties obtained by applying the correlations in Equation 7

that uses the renewable jet fuel chemical constituent amounts determined by applying Equation

6. Table 4 shows the ranges of phenol fractional conversions in Reactions 1 and 7 in Equation

891   5, required to meet the ASTM D7566 standard for the renewable jet fuel product. Their feasible

892   ranges as shown in Table 4 are decided iteratively using Equations 6 and 7. The renewable jet

893   fuel product concentration determined by Equation 6 is applied in Equation 7 to determine the

894   product properties. The molar flows (in kmolph) of the renewable jet fuel constituent chemicals

895   obtained by applying the mass balance Equation 6 and their molar masses are: 1-tridecene

896   (11.4), methylcyclohexane (4.4), 2,5-xylenol (4.2), n-heptane (4), cis-decalin (1.5), 1-*trans*-

897   3,5-trimethylcyclohexane (1.2), diamantane (1.1), n-propylcyclohexane (1.04), 3,3,5-

898   trimethylheptane (0.93), 1,2-dimethyl-3-ethylbenzene (0.82), 1,2,3-trimethylbenzene (0.3),

899   1,2,3,4-tetrahydronaphthalene (0.24), diphenyl (0.12), n-butylcyclohexane (0.11), 1,2,4-

900   triethylbenzene (0.084), p-xylene (0.07), and bicyclohexyl (0.064).

901   Table 5. Renewable jet fuel properties estimated using the correlations in Equation 7 using the

902   concentration determined by Equation 6, based on the default values shown in Table 4.

| Specific gravity	0.81
Aromatics volume %	21.3
Hydrogen weight %	13.33
Cetane number	50
Aniline point ($^{\circ}$C)	53
Flash point ($^{\circ}$C)	56
Volumetric average boiling point ($^{\circ}$C)	183

903

904   The economic analysis parameters in Table 4 include installation factor, annual capital charge,

905   and price and cost data. Using the size-cost correlation parameters shown in Table 3, the total

906   delivered cost of equipment is estimated to be $14million for the mass flowrates shown in Fig.

907   4. The CHP, pyrolysis, PSA, steam reforming, MIEC, hydrodeoxygenation and hydrocracking,

908   and distillation and decanter units cost 35%, 25.2%, 17.4%, 13%, 7%, 2.2% and 0.2% of the

909 delivered cost of equipment (Fig. 6a). Fig. 6b shows the economic margin analysis comprising

910 product value, feedstock cost, annual capital cost and operating cost contributions, 54%, 20%,

911 17% and 9%, respectively. For the default values in Table 4 and resulted mass flowrates shown

912 in Fig. 4, the product value, feedstock cost, annual capital cost and operating cost in million $

913 per annum are 5.7, 2, 1.8 and 0.9, respectively. Thus, the annual income in million $ per annum

914 is $(5.7 - 2 - 0.9) = 2.6$ for a delivered cost of equipment of $14million, giving a return on

915 investment $(\frac{annual\ income}{capital\ investment} \times 100)$ of 19%.

916 The cost of production is the total annual cost incurred including the biomass cost, divided by

917 the mass flowrate of the biomass, as shown in Fig. 6c. The value on processing of renewable

918 jet fuel, char and steam are their market prices. The value on processing for the renewable jet

919 fuel product and char is greater than their cost of production, thus, these products give

920 economic marginal gain for the biorefinery system. For steam, its value on processing is lower

921 than its cost of production, and thus, it incurs a marginal loss. Individual product margins are

922 equal to the area bounded between the product's flowrate, and its value on processing and cost

923 of production, i.e. product flowrate times the difference between its value on processing and

924 cost of production. The net margin from the biorefinery system is the net area above the COP.

925

926 (a)

45

927

928   (b)

929
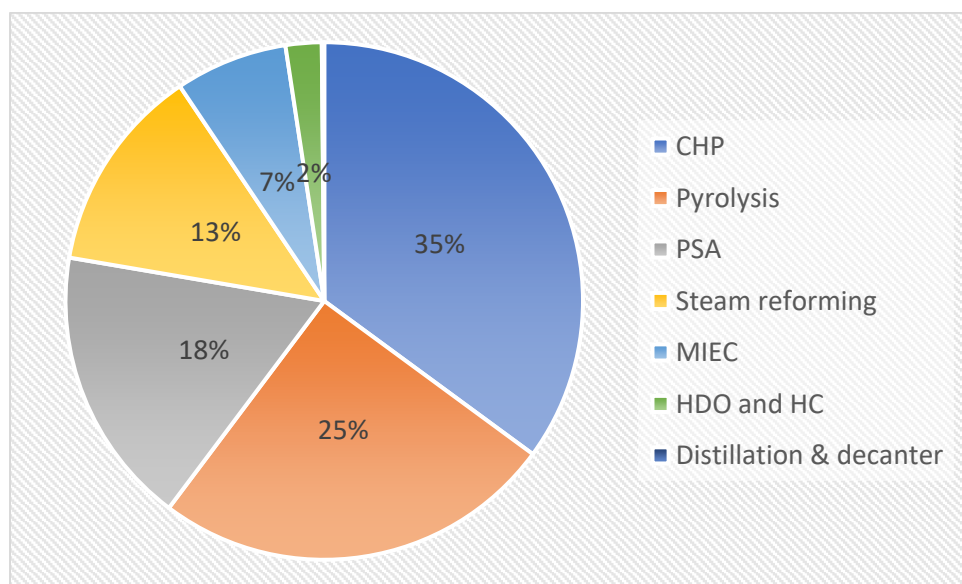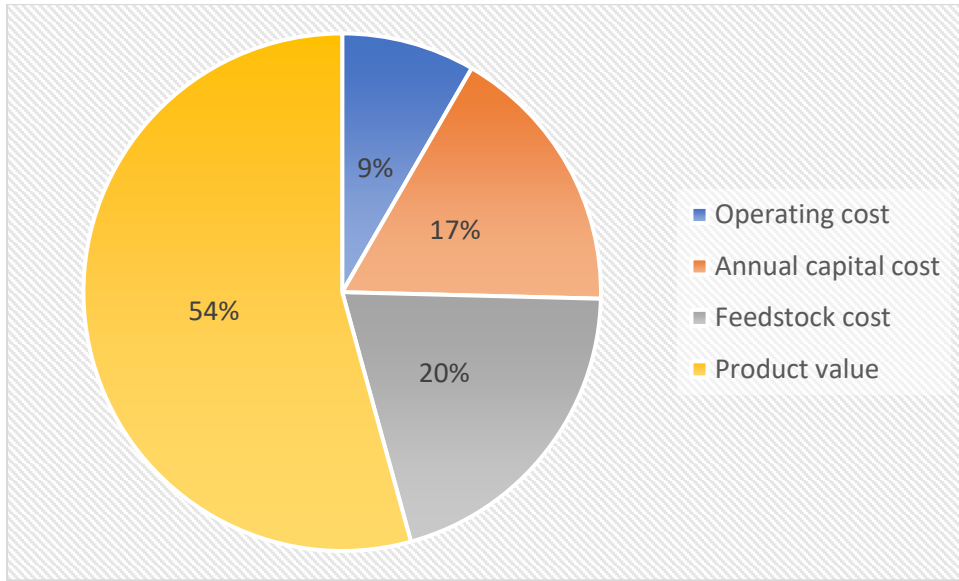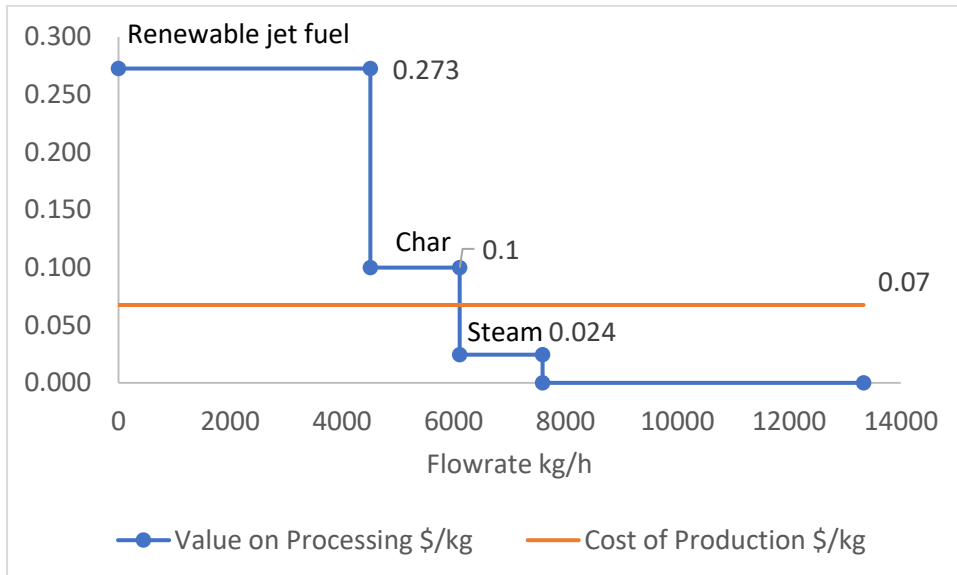
930   (c)

Fig. 6 (a) Capital cost contributions of the various unit processes in the biorefinery system in Fig. 1; (b) Economic marginal analysis of the biorefinery system in Fig. 1; (c) Value analysis of the outlet streams in the biorefinery system in Fig. 1.

Applying the global warming potential saving and fossil energy saving factors, the product renewable jet fuel (of 36 kt/y) is estimated to save 108 kt CO_2 equivalent per annum global warming potential and 1.44 PJ per annum fossil energy, by the displacement of conventional crude oil derived jet fuel.

938 The SHDB platform allows comparisons of mrh eq. for a given product between countries of

939 interest in each category. Here, a dimensionless ratio between mrh in business-as-usual import

940 case and mrh in a self-generation case for a given production rate is considered for each of the

941 SLCA impact categories to show the benefits or savings by indigenous energy security services

942 in social and socio-economic quantitative terms, compared to business as usual import cases.

943 The savings in the five main social impact categories are estimated for self-generation in the

944 UK compared to the present import scenario from the EU countries. In the decreasing order of

945 savings, the social impact categories are community infrastructure, governance, human rights,

946 health & safety, and labour rights & decent work, respectively. The relative social scores, i.e.

947 the ratio between mrh in the import scenario and mrh in self-generation, in five social categories

948 are estimated. These are 3.1, 2.1, 2, 1.3 and 1.1, in the five social impact categories,

949 respectively. The SHDB is a proprietary database with social scores (Benoît et al., 2010; Norris

950 et al., 2014). For this reason, relative scores are shown here. Savings mean better social

951 attributes, stressing the need for indigenous production of renewable jet fuel to meet the

952 country's demands.

953 **Conclusions**

954 The aviation sector is in desperate need of sustainable or renewable aviation fuels for

955 greenhouse gas negative or neutral performance. A very few pieces of literature have only

956 extended their studies beyond hydroprocessing into process integration. The previous studies

957 have only considered partial sourcing of hydrogen within biorefinery and/or purchasing of

958 hydrogen to meet its demand by hydroprocessing. Self-sustainability of a biorefinery is

959 imperative implies zero or least dependency on external supply to fulfil its in-process demands

960 for raw materials and utilities other than the biomass feedstock such as hydrogen, oxygen,

961 electricity, heat, etc. This research has advanced the biorefinery process integration concept to

962 think beyond the unit process. What one process cannot achieve; an overall integrated system

963 can achieve. The literature so far has focused on the reaction process, pyrolysis or

964 hydroprocessing. None has shown how to take the design from one step to multi-step to meet

965 *all* hydrogen, energy and oxygen requirements from the biomass feedstock itself. The processes

966 are inevitable to fail to meet economic or environmental criteria if they are to buy hydrogen or

967 energy and this is the present state of the art. This is the main bottleneck to the industrial uptake.

968 This research shows a compelling case by its inherent sustainability through process integration

969 for the industry. This research develops a novel integrated self-sustainable biorefinery system

970 to produce renewable aviation fuel. This research shows comprehensive mathematical

971 modelling equations for the design and sustainability evaluations of a novel integrated

972 biorefinery system producing renewable aviation fuel from biomass. It shows both the

973 systematic development of the integrated biorefinery system and the mathematical model for

974 design and sustainability evaluations of the system. The novel biorefinery system integrates

975 the following process units: 1) Fast pyrolysis converting waste biomass into pyrolysis gas, bio-

976 oil and char, 2) Bio-oil hydrodeoxygenation, decanting, distillation and hydrocracking to

977 renewable jet fuel product and alkanes for steam reforming, 3) Steam reforming of alkanes

978 from distillation into hydrogen production followed by hydrogen separation from offgas

979 containing carbon monoxide in PSA, 4) MIEC splitting high pressure superheated steam into

980 hydrogen, to meet remaining hydrogen demand by hydrodeoxygenation and hydrocracking,

981 and oxygen for CHP, 5) CHP comprising a boiler combusting pyrolysis gas and offgas from

982 PSA using oxygen from MIEC; the boiler turning medium pressure steam into the generation

983 of high pressure superheated steam (primarily for the alkane steam reforming and MIEC) by

984 heat of combustion of the gases, and a back pressure steam turbine turning some high pressure

985 superheated steam into electricity to meet site electricity demand. This research shows the mass

986 and energy balance analyses across the integrated biorefinery system, reaction kinetic

987 modelling of biomass pyrolysis, stoichiometric hydrodeoxygenation and hydrocracking

48

reaction modelling, and renewable jet fuel property correlations from its constituent chemical compositions. These enable biorefinery design evaluations without the use of proprietary process simulation packages (See TESARREC™ https://tesarrec.web.app/sustainability/bio-jet-fuel). Such open-source platform is helpful for designers, decision-makers, and policymakers to rapidly and effectively analyse biorefinery systems. This conceptual analysis can lead to the FEED stage for interested parties. The products from the biorefinery system (based on 1.33 mass units of biomass) are renewable jet fuel (0.45), char (0.16) and excess medium pressure steam (0.148). The energy outputs from the biorefinery system relative to the biomass energy input, are renewable jet fuel product (0.7), char (0.14) and excess medium pressure steam (0.016). Thus, the overall biorefinery energy efficiency is 85.6%. The renewable jet fuel properties relevant for the ASTM D7566 are specific gravity (0.81), aromatics volume (21.3%), hydrogen weight (13.33%), cetane number (50), aniline point (53°C), flash point (56°C) and volumetric average boiling point (183°C). The main components (%mol) of sustainable aviation fuel controlling the ASTM D7566 properties are: 1-tridecene (35.8), methylcyclohexane (13.8), 2,5-xylenol (13.4), n-heptane (12.8), cis-decalin (4.8), 1-trans-3,5-trimethylcyclohexane (4), diamantane (3.5), n-propylcyclohexane (3.3), 3,3,5-trimethylheptane (2.9), 1,2-dimethyl-3-ethylbenzene (2.6), 1,2,3-trimethylbenzene (0.98), 1,2,3,4-tetrahydronaphthalene (0.76), diphenyl (0.38), n-butylcyclohexane (0.34), 1,2,4-triethylbenzene (0.27), p-xylene (0.22), and bicyclohexyl (0.2). Thus, these chemicals can be targeted from biomass for renewable fuel production. The techno-economic analysis gives a delivered cost of equipment of \$14m for a bio-oil throughput of 10 tph, and \$2.8m for a bio-oil throughput of 1 tph. The return on investment is estimated to be 19%. The techno-economic analysis also shows attributions of product value, and feedstock, annual capital and operating costs of 54%, 20%, 17% and 9%, respectively. In decreasing order of capital costs, the units are CHP (35%), pyrolysis (25.2%), PSA (17.4%), steam reforming (13%), MIEC (7%),

hydrodeoxygenation and hydrocracking (2.2%), and distillation and decanter (0.2%), respectively. The value analysis shows the cost of production of $0.07/kg for a bio-oil throughput of 10 tph, in comparison to the market prices of the products, $0.273, $0.1 and $0.024 per kg renewable jet fuel, char and steam. A renewable jet fuel yield of 4.5 tph (34% by mass of biomass) based on 10 tph bio-oil throughput could potentially save 108 kt CO_2 equivalent per annum global warming and 1.44 PJ/a fossil energy by displacement of conventional jet fuel. Social life cycle assessment reinstates the significance of self-generation in improving indigenous social conditions. In decreasing order of the ratio of mrh between import and self-generation cases, the categories are community infrastructure (3.1), governance (2.1), human rights (2), health & safety (1.3), and labour rights & decent work (1.1). The above performance indicators show that the novel integrated biorefinery design is sustainable.

References

Arratibel Plazaola, A., Cruellas Labella, A., Liu, Y., Badiola Porras, N., Pacheco Tanaka, D.A., Sint Annaland, M.V., Gallucci, F., 2019. Mixed ionic-electronic conducting membranes (MIEC) for their application in membrane reactors: a review. Processes 7(3), 128.

ASTM D7566-20c, Standard Specification for Aviation Turbine Fuel Containing Synthesized Hydrocarbons, ASTM International, West Conshohocken, PA, 2020. www.astm.org

BEIS, 2021. https://www.gov.uk/government/collections/digest-of-uk-energy-statistics-dukes#2021

Benoît, C., Norris, G.A., Valdivia, S., Ciroth, A., Moberg, A., Bos, U., Prakash, S., Ugaya, C., Beck, T., 2010. The guidelines for social life cycle assessment of products: just in time! Int. J. Life Cycle Assess. 15(2), 156-163.

1037   Cai, J., He, Y., Yu, X., Banks, S.W., Yang, Y., Zhang, X., Yu, Y., Liu, R., Bridgwater, A.V.,

1038   2017. Review of physicochemical properties and analytical characterization of

1039   lignocellulosic biomass. Renew. Sustain. Energy Rev. 76, 309-322.

1040   COP26, 2021. https://ukcop26.org/

1041   Dimian, A.C., Bildea, C.S. and Kiss, A.A., 2014. Integrated Design and Simulation of

1042   Chemical Processes. Elsevier.

1043   Ebikade, E., Athaley, A., Fisher, B., Yang, K., Wu, C., Ierapetritou, M.G. and Vlachos, D.G.,

1044   2020. The future is garbage: repurposing of food waste to an integrated biorefinery. ACS

1045   Sustain. Chem. Eng. 8(22), 8124-8136.

1046   El-Halwagi, M.M., 2017. Sustainable design through process integration: fundamentals and

1047   applications to industrial pollution prevention, resource conservation, and profitability

1048   enhancement. Butterworth-Heinemann.

1049   EU RED, 2018. Directive (EU) 2018/2001 of The European Parliament and of The Council,

1050   2018.   https://eur-lex.europa.eu/legal-

1051   content/EN/TXT/?uri=uriserv:OJ.L_.2018.328.01.0082.01.ENG

1052   Geffroy, P.M., Fouletier, J., Richet, N., Chartier, T., 2013. Rational selection of MIEC

1053   materials in energy production processes. Chem. Eng. Sci. 87, 408-433.

1054   Gutiérrez-Antonio, C., Romero-Izquierdo, A.G., Gómez-Castro, F.I. and Hernández, S., 2020.

1055   Production Processes of Renewable Aviation Fuel, Elsevier.

1056   Harvey, B.G., Merriman, W.W. and Koontz, T.A., 2015. High-density renewable diesel and jet

1057   fuels prepared from multicyclic sesquiterpanes and a 1-hexene-derived synthetic paraffinic

1058   kerosene. Energy Fuels 29(4), 2431-2436.

1059   Jahirul, M.I., Rasul, M.G., Chowdhury, A.A., Ashwath, N., 2012. Biofuels production through

1060   biomass pyrolysis—a technological review. Energies 5(12), 4952-5001.

Ji, Q., Bi, L., Zhang, J., Cao, H., Zhao, X.S., 2020. The role of oxygen vacancies of ABO 3 perovskite oxides in the oxygen reduction reaction. Energy Environ. Sci. 13(5), 1408-1428.

Jones, S.B., Valkenburt, C., Walton, C.W., Elliott, D.C., Holladay, J.E., Stevens, D.J., Kinchin, C., Czernik, S., 2009. Production of gasoline and diesel from biomass via fast pyrolysis, hydrotreating and hydrocracking: a design case (No. PNNL-18284 Rev. 1). Pacific Northwest National Lab. (PNNL), Richland, WA (United States).

Kolios, G., Glöckler, B., Gritsch, A., Morillo, A., Eigenberger, G., 2005. Heat-integrated reactor concepts for hydrogen production by methane steam reforming. Fuel Cells 5(1), 52-65.

Kolosz, B.W., Luo, Y., Xu, B., Maroto-Valer, M.M., Andresen, J.M., 2020. Life cycle environmental analysis of 'drop in' alternative aviation fuels: a review. Sustain. Energy Fuels 4(7), 3229-3263.

Leong, H., Leong, H., Foo, D.C., Ng, L.Y. and Andiappan, V., 2019. Hybrid approach for carbon-constrained planning of bioenergy supply chain network. Sustain. Prod. Consump. 18, 250-267.

Li, W., Cao, Z., Zhu, X., Yang, W., 2017. High-rate hydrogen separation using an MIEC oxygen permeable membrane reactor. AIChE J. 63(4), 1278-1286.

Liden, A.G., Berruti, F., Scott, D.S., 1988. A kinetic model for the production of liquids from the flash pyrolysis of biomass. Chem. Eng. Comm. 65(1), 207-221.

Ling, W.C., Verasingham, A.B., Andiappan, V., Wan, Y.K., Chew, I.M. and Ng, D.K., 2019. An integrated mathematical optimisation approach to synthesise and analyse a bioelectricity supply chain network. Energy 178, 554-571.

Liu, S., Dutta, S., Zheng, W., Gould, N.S., Cheng, Z., Xu, B., Saha, B. and Vlachos, D.G., 2017. Catalytic hydrodeoxygenation of high carbon furylmethanes to renewable jet-fuel

ranged alkanes over a rhenium-modified iridium catalyst. ChemSusChem 10(16), 3225-3234.

Martinez-Hernandez, E., Campbell, G.M., Sadhukhan, J., 2013. Economic value and environmental impact (EVEI) analysis of biorefinery systems. Chem. Eng. Res. Des. 91(8), 1418-1426.

Martinez-Hernandez, E., Campbell, G.M., Sadhukhan, J., 2014. Economic and environmental impact marginal analysis of biorefinery products for policy targets. J. Cleaner Product. 74, 74-85.

Martinez-Hernandez, E., Ramírez-Verduzco, L.F., Amezcua-Allieri, M.A., Aburto, J., 2019. Process simulation and techno-economic analysis of bio-jet fuel and green diesel production—Minimum selling prices. Chem. Eng. Res. Des. 146, 60-70.

Martinez, I., 2021. Fuel Properties. http://webserver.dmt.upm.es/~isidoro/bk3/c15/Fuel%20properties.pdf

Mofijur, M., Mahlia, T.M.I., Logeswaran, J., Anwar, M., Silitonga, A.S., Rahman, S.M. and Shamsuddin, A.H., 2019. Potential of rice industry biomass as a renewable energy source. Energies 12(21), p.4116.

Musa, S.H., 2017. Potential application of pyrolysis bio-oil as a substitute for diesel and petroleum fuel. Forest 69(61.2), 19.

Nanda, S., Azargohar, R., Dalai, A.K., Kozinski, J.A., 2015. An assessment on the sustainability of lignocellulosic biomass for biorefining. Renew. Sustain. Energy Rev. 50, 925-941.

Ng, D.K., Tan, R.R., Foo, D.C., El-Halwagi, M.M., 2015. Process Design Strategies for Biomass Conversion Systems. John Wiley & Sons.

Ng, K.S., Sadhukhan, J., 2011. Techno-economic performance analysis of bio-oil based Fischer-Tropsch and CHP synthesis platform. Biomass Bioenergy 35(7), 3218-3234.

Norris, C.B., Norris, G.A., Aulisio, D., 2014. Efficient assessment of social hotspots in the supply chains of 100 product categories using the social hotspots database. Sustain. 6(10), 6973-6984.

Popp, J., Lakner, Z., Harangi-Rakos, M., Fari, M., 2014. The effect of bioenergy expansion: Food, energy, and environment. Renew. Sustain. Energy Rev. 32, 559-578.

Raja, M.W., Islam, Q.A., Basu, R.N., 2017. Oxygen separation membrane derived from aquatic weed: A novel bio-inspired approach to synthesize $BaBi_{0.2}Co_{0.35}Fe_{0.45}O_{3-\delta}$ perovskite from water hyacinth (Eichhornia crassipes). J. Membrane Sci. 522, 168-174.

Ranzi, E., Debiagi, P.E.A. and Frassoldati, A., 2017. Mathematical modeling of fast biomass pyrolysis and bio-oil formation. Note II: secondary gas-phase reactions and bio-oil formation. ACS Sustain. Chem. Eng. 5(4), pp.2882-2896.

Riboldi, L., Bolland, O., 2016. Pressure swing adsorption for coproduction of power and ultrapure H2 in an IGCC plant with CO2 capture. Int. J. Hydrogen Energy 41(25), 10646-10660.

Risch, M., 2017. Perovskite electrocatalysts for the oxygen reduction reaction in alkaline media. Catalysts 7(5), 154.

Romero-Izquierdo, A.G., Gómez-Castro, F.I., Gutiérrez-Antonio, C., Hernández, S. and Errico, M., 2021. Intensification of the alcohol-to-jet process to produce renewable aviation fuel. Chem. Eng. Processing-Process Intensification 160, 108270.

Sadhukhan, J., Dugmore, T.I., Matharu, A., Martinez-Hernandez, E., Aburto, J., Rahman, P.K. and Lynch, J., 2020. Perspectives on "game changer" global challenges for sustainable 21st century: plant-based diet, unavoidable food waste biorefining, and circular economy. Sustain. 12(5), p.1976.

Sadhukhan, J., Gadkari, S., Martinez-Hernandez, E., Ng, K.S., Shemfe, M., Torres-Garcia, E., Lynch, J., 2019. Novel macroalgae (seaweed) biorefinery systems for integrated chemical,

protein, salt, nutrient and mineral extractions and environmental protection by green synthesis and life cycle sustainability assessments. Green Chem. 21(10), 2635-2655.

Sadhukhan, J., Martinez-Hernandez, E., Murphy, R.J., Ng, D.K., Hassim, M.H., Ng, K.S., Kin, W.Y., Jaye, I.F.M., Hang, M.Y.L.P., Andiappan, V., 2018. Role of bioenergy, biorefinery and bioeconomy in sustainable development: Strategic pathways for Malaysia. Renew. Sustain. Energy Rev. 81, 1966-1987.

Sadhukhan, J., Ng, K.S., 2011. Economic and European union environmental sustainability criteria assessment of bio-oil-based biofuel systems: refinery integration cases. Ind. Eng. Chem. Res. 50(11), 6794-6808.

Sadhukhan, J., Ng, K.S., Martinez-Hernandez, E., 2014. Biorefineries and Chemical Processes. Design, Integration and Sustainability Analysis. Wiley, UK.

Sadhukhan, J., Sen, S., Gadkari, S., 2021. The Mathematics of Life Cycle Sustainability Assessment. J. Cleaner Product. 309, 127457.

Sen, S. 2020. https://github.com/sohumsen/Tesarrec/blob/master/src/components/Calculations/Sustainability/BioJetFuel/BioJetFuel.js

Shemfe, M.B., Gadkari, S., Sadhukhan, J., 2018. Social hotspot analysis and trade policy implications of the use of bioelectrochemical systems for resource recovery from wastewater. Sustain. 10(9), 3193.

Sy, C.L., Ubando, A.T., Aviso, K.B., Tan, R.R., 2018. Multi-objective target oriented robust optimization for the design of an integrated biorefinery. J. Cleaner Product. 170, 496-509.

TESARREC[TM] Trademark: UK00003321198, 2018. S. Sen, 2020. https://tesarrec.web.app/; https://tesarrec.web.app/sustainability; https://tesarrec.web.app/sustainability/bio-jet-fuel; https://tesarrec.web.app/sustainability/pyrolysis; https://tesarrec.web.app/sustainability/chp

1161 Thursfield, A. and Metcalfe, I.S., 2004. The use of dense mixed ionic and electronic conducting

1162   membranes for chemical production. J. Materials Chem. 14(16), 2475-2485.

1163 Trogadas, P. and Coppens, M.O., 2020. Nature-inspired electrocatalysts and devices for energy

1164   conversion. Chem. Soc. Rev. 49(10), 3107-3141.

1165 UN Comtrade Database, 2019. https://comtrade.un.org/data/

1166 Wang, Z., Bhattacharyya, S. and Vlachos, D.G., 2021. Extraction of Furfural and Furfural/5-

1167   Hydroxymethylfurfural from Mixed Lignocellulosic Biomass-Derived Feedstocks. ACS

1168   Sustain. Chem. Eng.

1169 Yang, X., Zhao, Y., Li, R., Wu, Y., Yang, M., 2018. A modified kinetic analysis method of

1170   cellulose pyrolysis based on TG–FTIR technique. Thermochimica acta 665, 20-27.

1171 Zacher, A.H., Olarte, M.V., Santosa, D.M., Elliott, D.C. and Jones, S.B., 2014. A review and

1172   perspective of recent bio-oil hydrotreating research. Green Chem. 16(2), 491-515.

1173 Zhang, L., Butler, T.L. and Yang, B., 2020. Recent Trends, Opportunities and Challenges of

1174   Sustainable Aviation Fuel. Green Energy to Sustainability: Strategies for Global

1175   Industries, 85-110.

1176 **Appendix A**
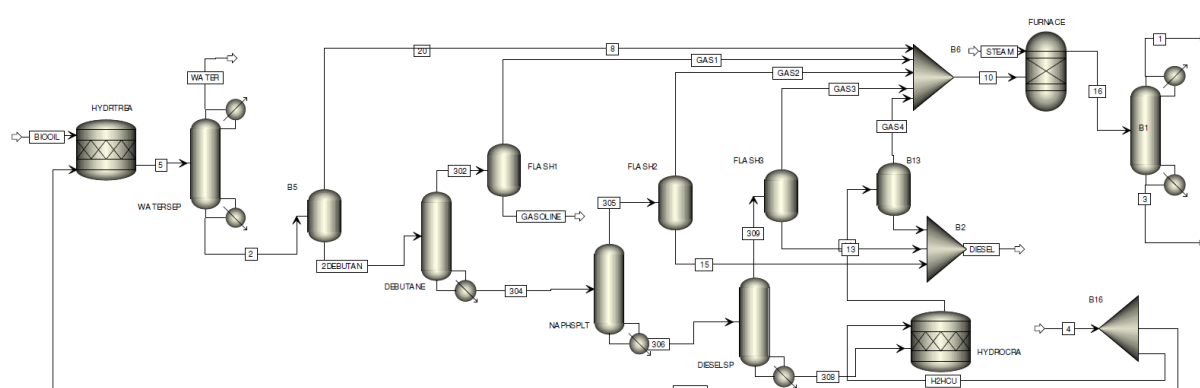
1178 **Fig. A1** Simulation schematic of a hydrodeoxygenation reactor (HYDROTREA), a decanter

1179 (WATERSEP), reboiler distillation columns (DEBUTANE, NAPHSPLT and DIESELSP)

1180 with top flash columns (FLASH1-3), a hydrocracking reactor (HYDROCRA) with a flash

column (B13), a steam reformer (FURNACE), and a PSA (B1). The process simulated on Aspen Plus is discussed as follows (Sadhukhan and Ng, 2011).

The Reactions 1-36 in Equation 5 are for the hydrodeoxygenation reactor (HYDROTREA in Fig. A1) and the Reactions 37-40 in Equation 5 are for the hydrocracking reactor (HYDROCRA in Fig. A1), respectively. The operating conditions of hydrodeoxygenation are 150-250°C and 170 bar and of hydrocracking are 350-400°C and 85 bar. Excess hydrogen once sourced can be circulated around the system. Only the consumed hydrogen by the reactions in Equation 5 is needed to be produced within the system. The distillation columns have been simulated as reboiler columns requiring no condenser (DEBUTANE, NAPHSPLT and DIESELSP in Fig. A1), each with a side flash column (FLASH1-3 in Fig. A1). The pressure of the flash and distillation columns varies between atmospheric and 3.5 bar. The hydrocracker reactor outlet also goes to another flash column (B13 in Fig. A1). These flash columns separate light alkanes as feedstock to steam reformer (FURNACE in Fig. A1) from the bottom fraction pool directed to the hydrocracking reactor. A decanter (WATERSEP in Fig. A1) and a flash column (B5 in Fig. A1) are needed after the hydrodeoxygenation reactor and before the distillation columns to separate steam (medium pressure) (WATER in Fig. A1) and gas from liquid hydrocarbon feed to the distillation columns. This medium pressure steam is a hydrodeoxygenation reaction product. Steam reforming of alkanes produces hydrogen and carbon monoxide (FURNACE in Fig. A1). PSA (B1 in Fig. A1) is applied to separate hydrogen from carbon monoxide rich offgas. Hydrogen produced from the steam reformer and separated from CO-rich offgas in PSA is used in the hydrodeoxygenation and hydrocracking reactors (H2HTU and H2HCU streams in Fig. A1). The final renewable jet fuel is the pool of GASOLINE and DIESEL in Fig. A1 from the bottom of the side flash columns.